Supporting Information

New Reactions of Terminal Hydrides on a Diiron Dithiolate

Wenguang Wang, Thomas B. Rauchfuss*, Lingyang Zhu, Giuseppe Zampella*

Part I. Spectra

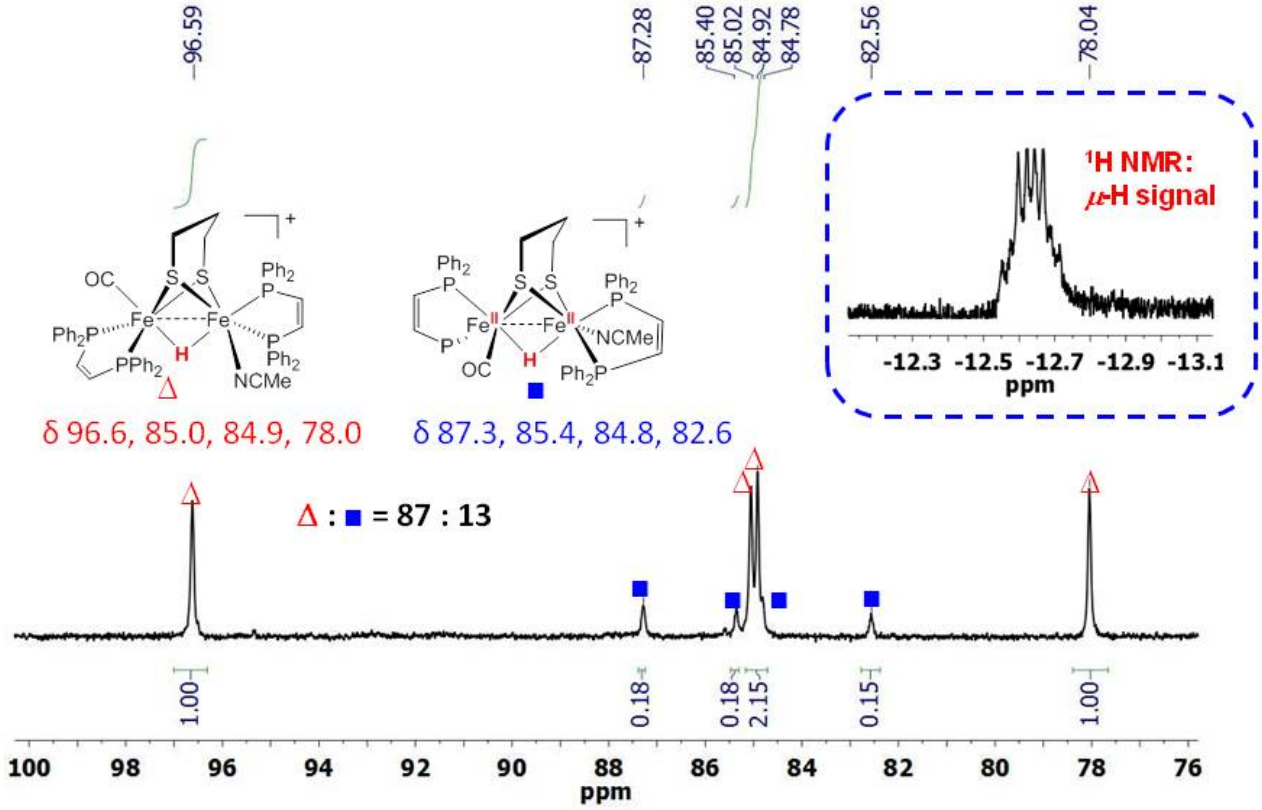

Figure S1. $^{31}P\ \{^{1}H\}$ NMR spectrum of $[HFe_2(pdt)(CO)(NCMe)(dppv)_2]BF_4$ in CH_2Cl_2 solution. The ratio of two isomers ab-bb/ab-ab is 87:13. *Insert:* ^{1}H NMR signal of the bridging hydride signal at δ -12.68 for the major isomer.

Assignments:

δ 96.6 (s), 85 (s), 84.9 (s) and 78 (s) = ab-bb isomer.

δ 87.3 (s), 85.4 (s), 84.8 (s) and 82.6 (s) = ab-ab isomer.

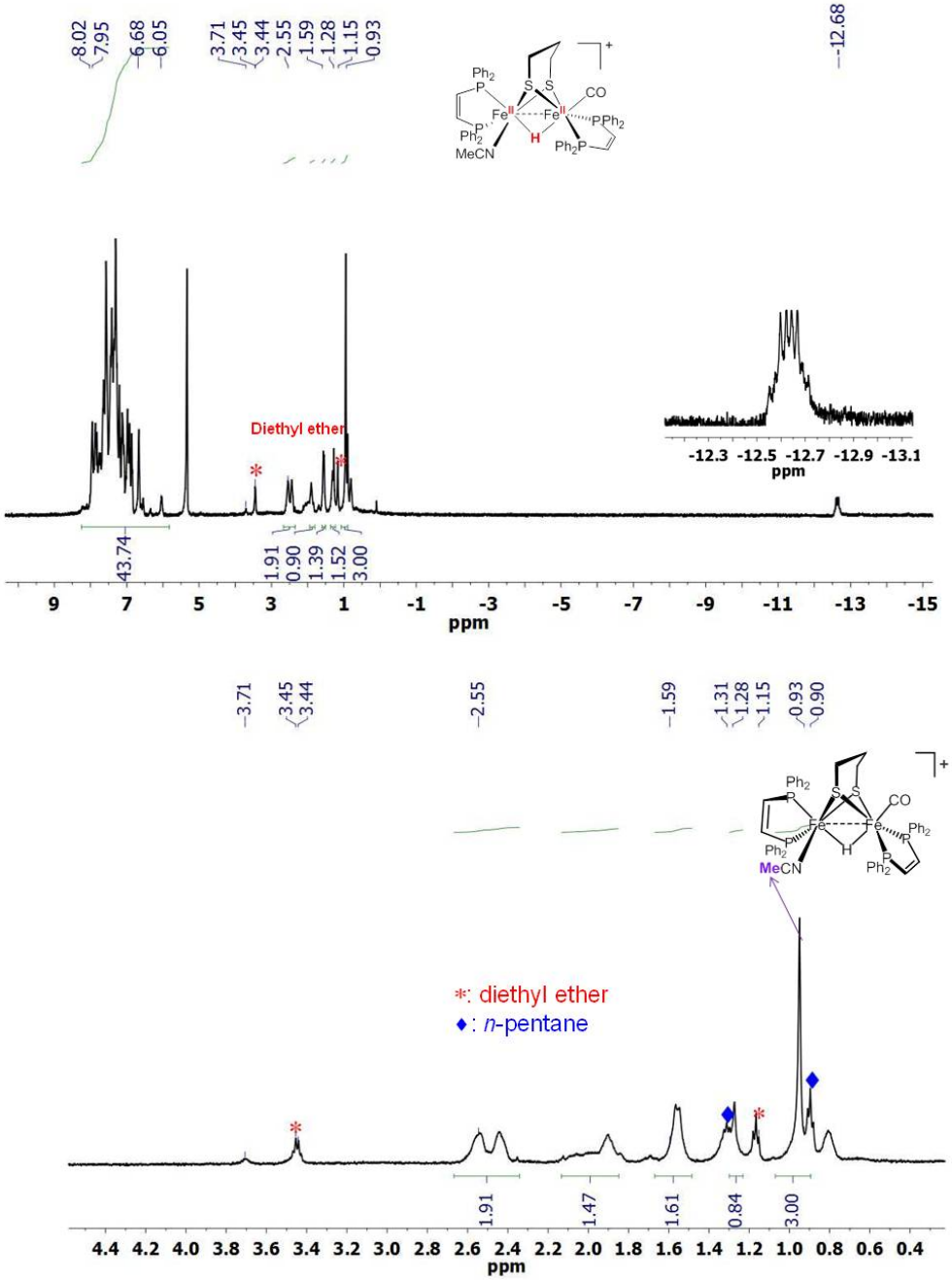

Figure S2. ^{1}H NMR spectrum of $[HFe_2(pdt)(CO)(NCMe)(dppv)_2]BF_4$ in CH_2Cl_2 solution.

Assignments: δ 8.02-6.05 (m, 44H, 40 × Ar*H*, 2 × Ph_2PC*H*=C*H*PPh_2), 2.55-1.15 (m, 6H, SC*H*$_2C$*H*$_2SC$*H*$_2$), 0.93 (s, 3H, CH_3CN), −12.68 (m, 1H, μ-H). Lower: expanded view below.

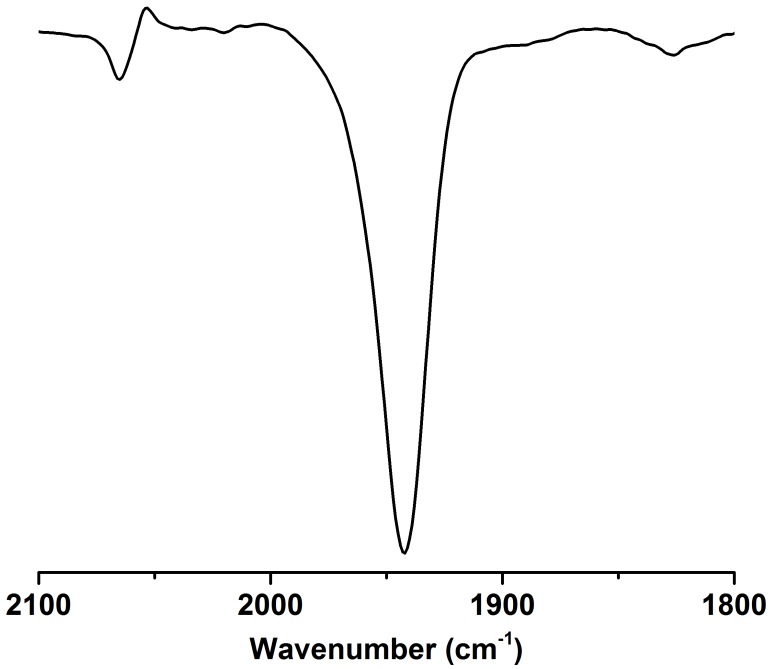

Figure S3. IR spectrum (ν_{CO} region, cm^{-1}) of $[DFe_2(pdt)(CO)(NCMe)(dppv)_2]PF_6$ ($[D\mathbf{1}(NCMe]^+$) in CH_2Cl_2 solution.
Results: ν_{CO} = 1942 cm^{-1}, which is the same as that in $[H\mathbf{1}(NCMe]^+$.

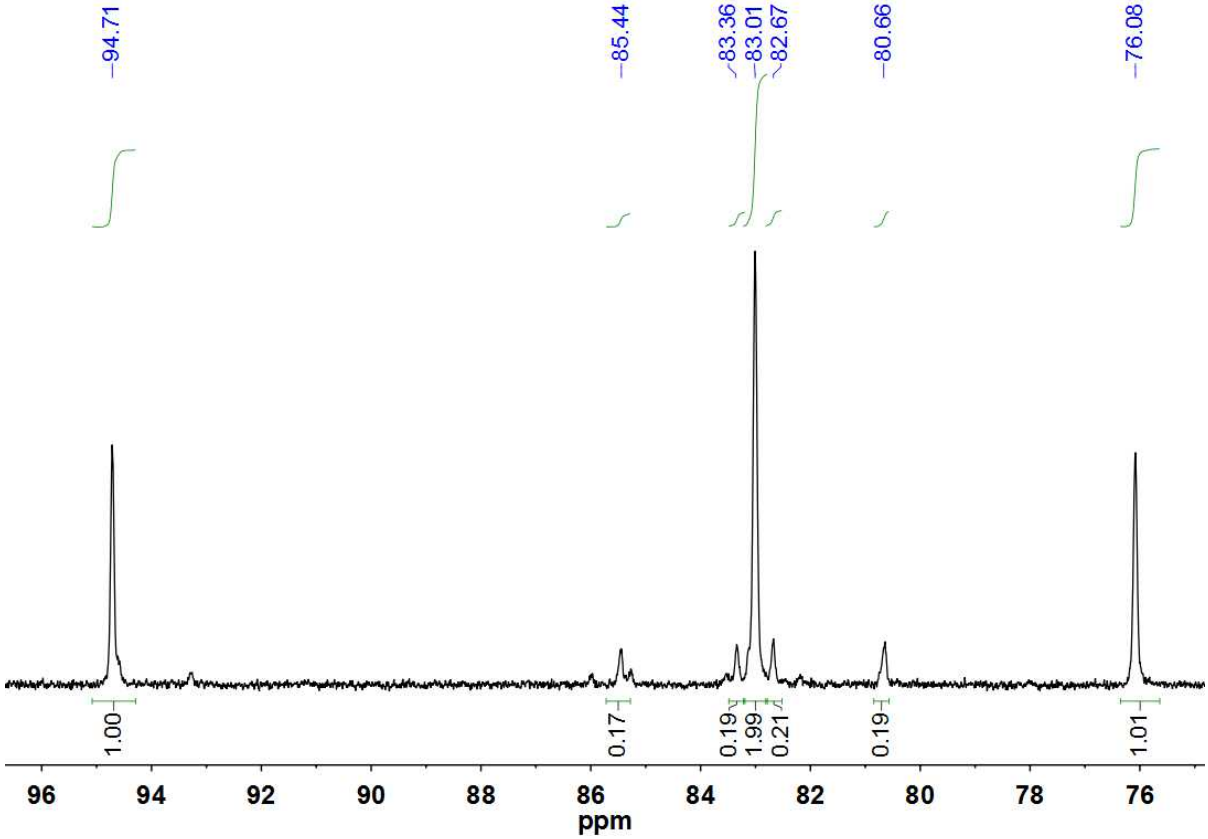

Figure S4. $^{31}P\{^{1}H\}$ NMR spectrum of $[DFe_2(pdt)(CO)(NCMe)(dppv)_2]BF_4$ in CH_2Cl_2 solution.

Assignments:

δ 94.7(s), 83(s), 76 (s) (ratio of 1:2:1) = ab-bb isomer (two signals at δ83)

δ 85.4(s), 83.4(s), 82.7 (s), 80.6 (s) = ab-ab isomer

other signals, e.g. near δ 86 are unassigned impurities

The ratio of two isomers ab-bb/ab-ab is 85:15

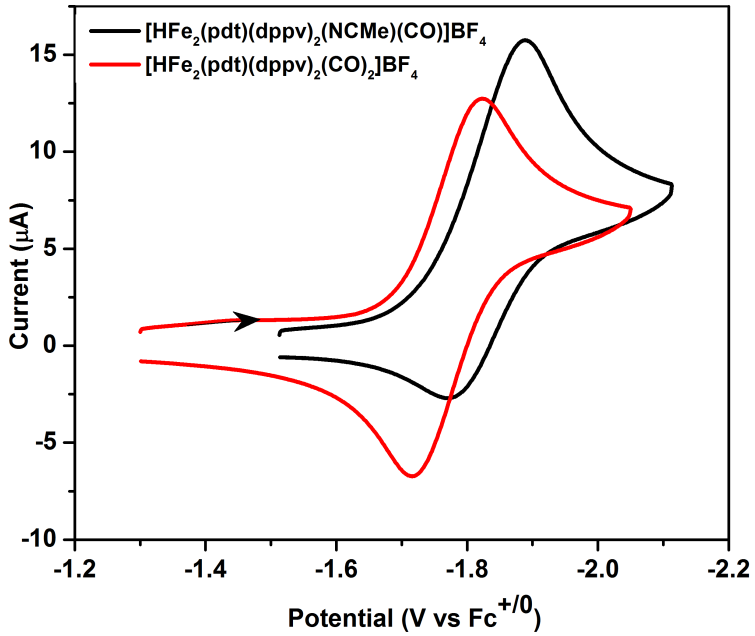

Figure S5. Cyclic votammograms for $[HFe_2(pdt)(dppv)_2(CO)_2]BF_4$ and $[HFe_2(pdt)(dppv)_2(NCMe)(CO)]BF_4$. Conditions: 10 mM sample in THF, 0.1 M Bu_4NPF_6; scan rate, 100 mV s^{-1}; potentials vs $Fc^{+/0}$. Results: $E_{1/2}[HFe_2(pdt)(dppv)_2(CO)_2]^{+/0}$ = − 1.77 V, i_{pc}/i_{pa} = 0.99; $E_{1/2}[HFe_2(pdt)(dppv)_2(NCMe)(CO)]^{+/0} = -1.83$V, $i_{pc}/i_{pa} = 0.47$.

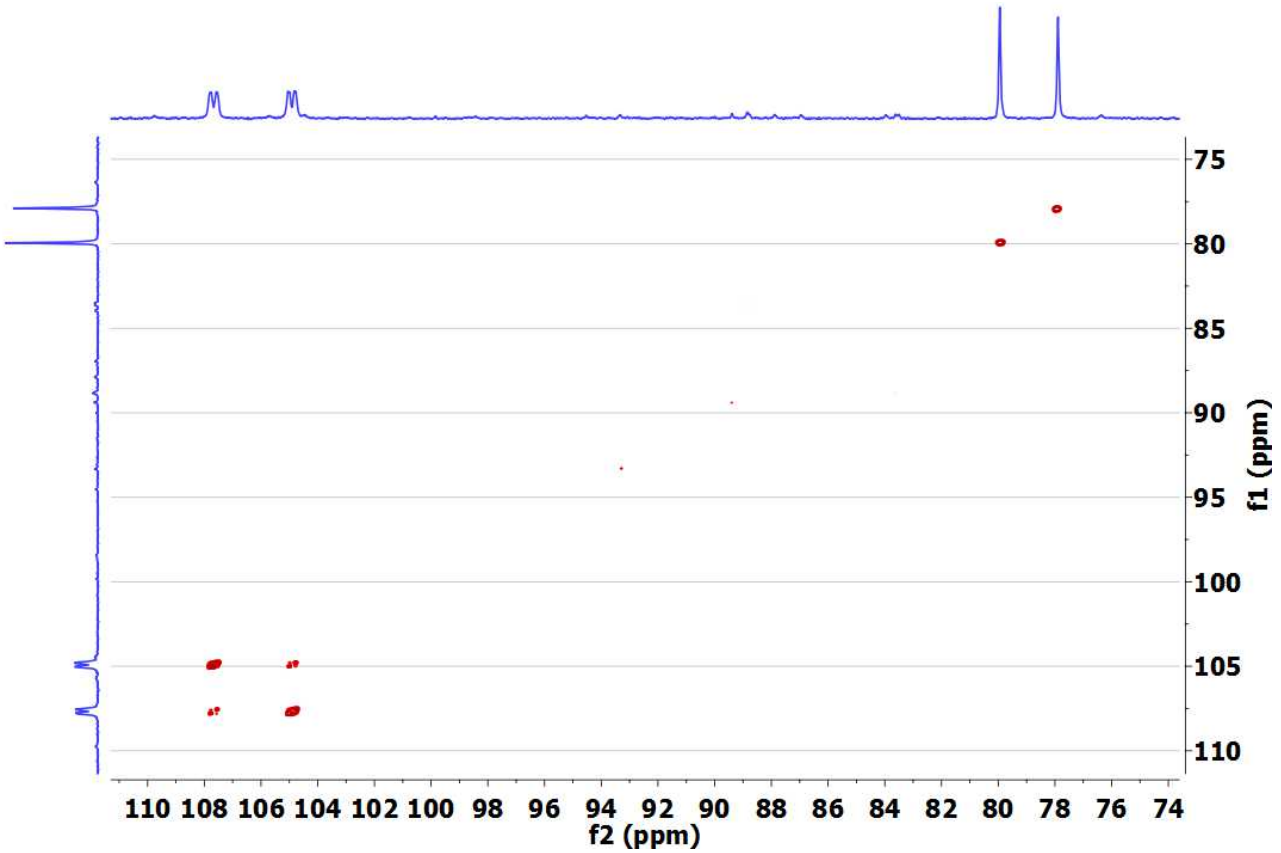

Figure 6. 2D ^{31}P-^{31}P TOCSY spectrum of [H**1**H]^{0} in THF-d_8 solution at -40 ºC with a mixing time of 40 ms.
Results: signals at δ108 (d), 105 (d) are coupled ($J_{P\text{-}P}$ = 56.5 Hz) and are assigned apical-basal dppv. No coupling is observed for the two signals assigned to dibasal dppv.

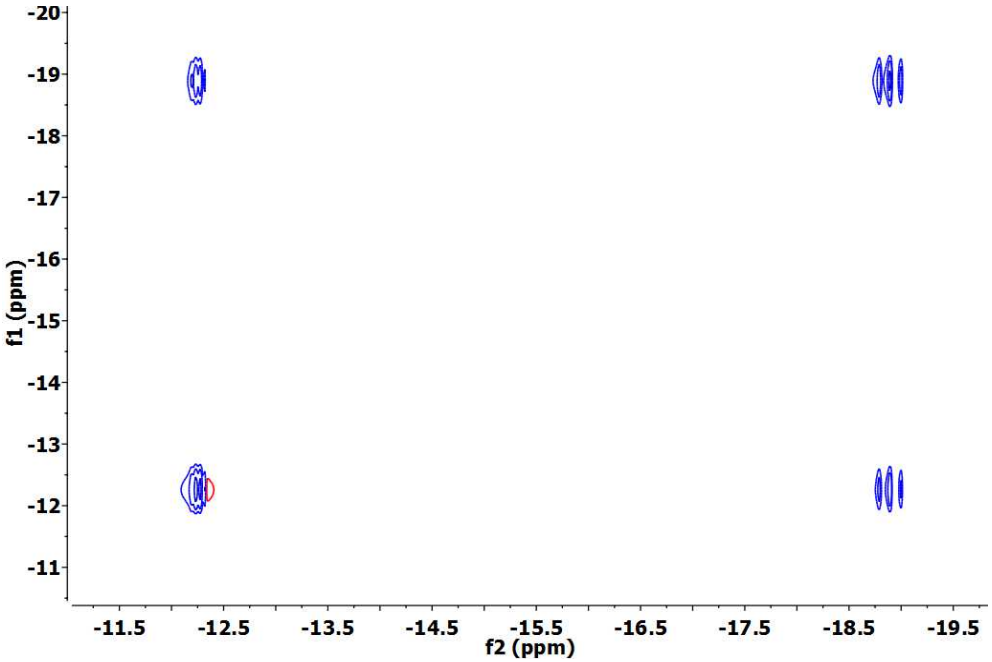

Figure S7. (^{1}H,^{1}H) EXSY spectrum (hydride region) of [H**1**H]^0 in THF-d_8 solution at -40 ºC with a mixing time of 500 ms. The cross-peaks from exchange are of the same phase (blue color) as the diagonal peaks.

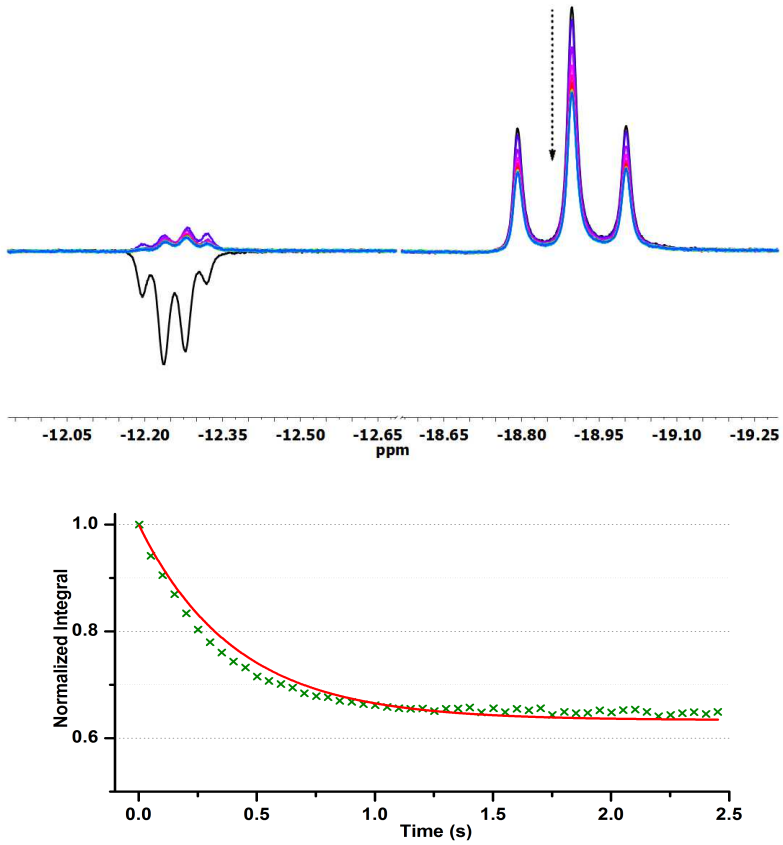

Figure S8. Spin saturation transfer spectra of $[H\mathbf{1}H]^0$ at -40 ºC in THF-d_8 solution (sample concentration, 24 mM), showing the decline in intensity of the hydride signal at δ -18.90 at longer irradiation time for the hydride resonance at δ -12.24 (top), and the plot of decay vs. time at δ -18.89 (bottom). The presaturation times increase by 0.05 s for each successive peak. Fitting results: $A_t/A_0 = 1/(1 + \tau/0.644) \times \exp[-t \times (1/0.644 + 1/\tau)] + 1/(1 + 0.644/\tau)$, $\tau = 1.10$ (standard error 0.0104), $k = 1/\tau = 0.91\ s^{-1}$.

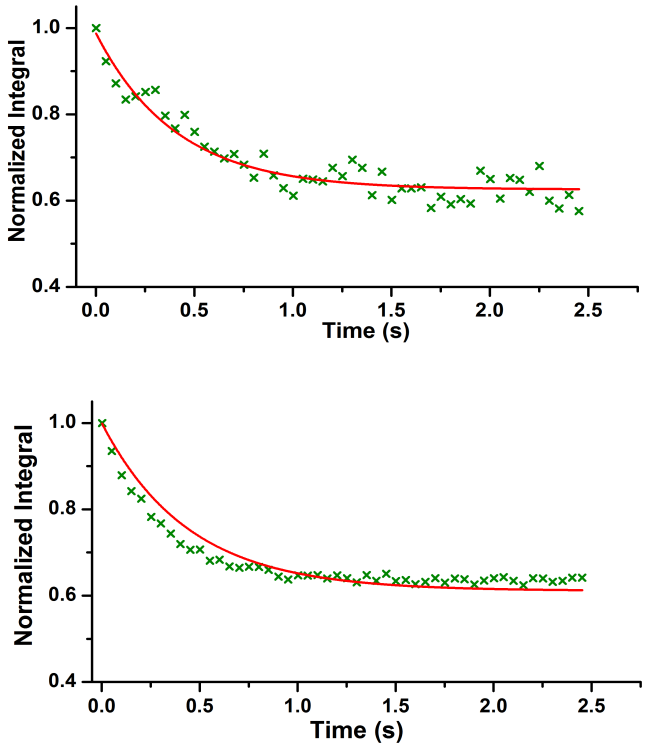

Figure S9. Spin saturation transfer spectra of $[H\mathbf{1}H]^0$ at -40 ºC in THF-d_8 solution with sample concentration of 8 mM.

Top: the plot of decay vs. presaturation time at δ -12.24, $A_t/A_0 = 1/(1 + \tau/0.641) \times \exp[-t \times (1/0.641 + 1/\tau)] + 1/(1 + 0.641/\tau)$, and gives $\tau =$ 1.1053 s (standard error 0.0608) and $k = 1/\tau = 0.91\ s^{-1}$.

Bottom: the plot of decay vs. presaturation time at δ -18.89, $A_t/A_0 = 1/(1 + \tau/0.725) \times \exp[-t \times (1/0.725 + 1/\tau)] + 1/(1 + 0.725/\tau)$, and gives $\tau =$ 1.1396 s (standard error 0.018) and $k^{-1} = 1/\tau = 0.88\ s^{-1}$.

Interpretation: Combined with the results in Figure S6, the exchange of the hydrides is concentration independent and, therefore, intramolecular.

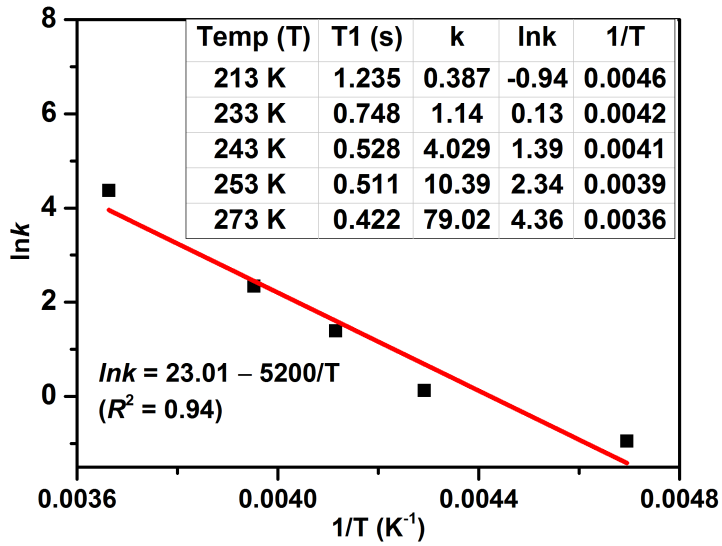

Figure S10. H/H exchange rates determined by SST experiments at various temperatures (insert), and plots of ln$k$ vs 1/T according to Arrhenius equation. Results: E_a = 43.2 kJ/mol,

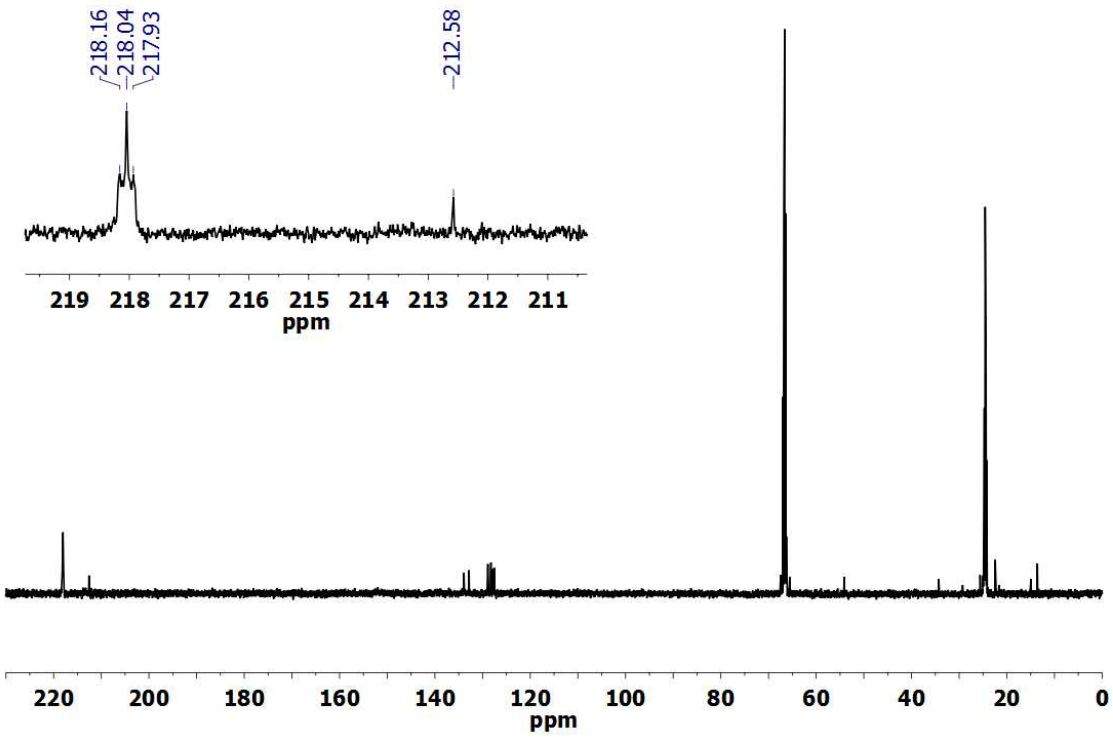

Figure S11. ^{13}C NMR spectrum for the reaction of $[H_2Fe_2(pdt)(dppv)_2(CO)]^0$ and $H(Et_2O)_2BAr^F{}_4$ in CH_2Cl_2 solution under ^{13}CO. *Insert:* Zoon in the spectrum in the CO region.

Assignment:

δ 218.4 (t, $J_{P\text{-}C}$ = 15 Hz), basal-^{13}CO at apicl-basal dppv site,

δ 212.6, apical CO at basal-basal dppv site

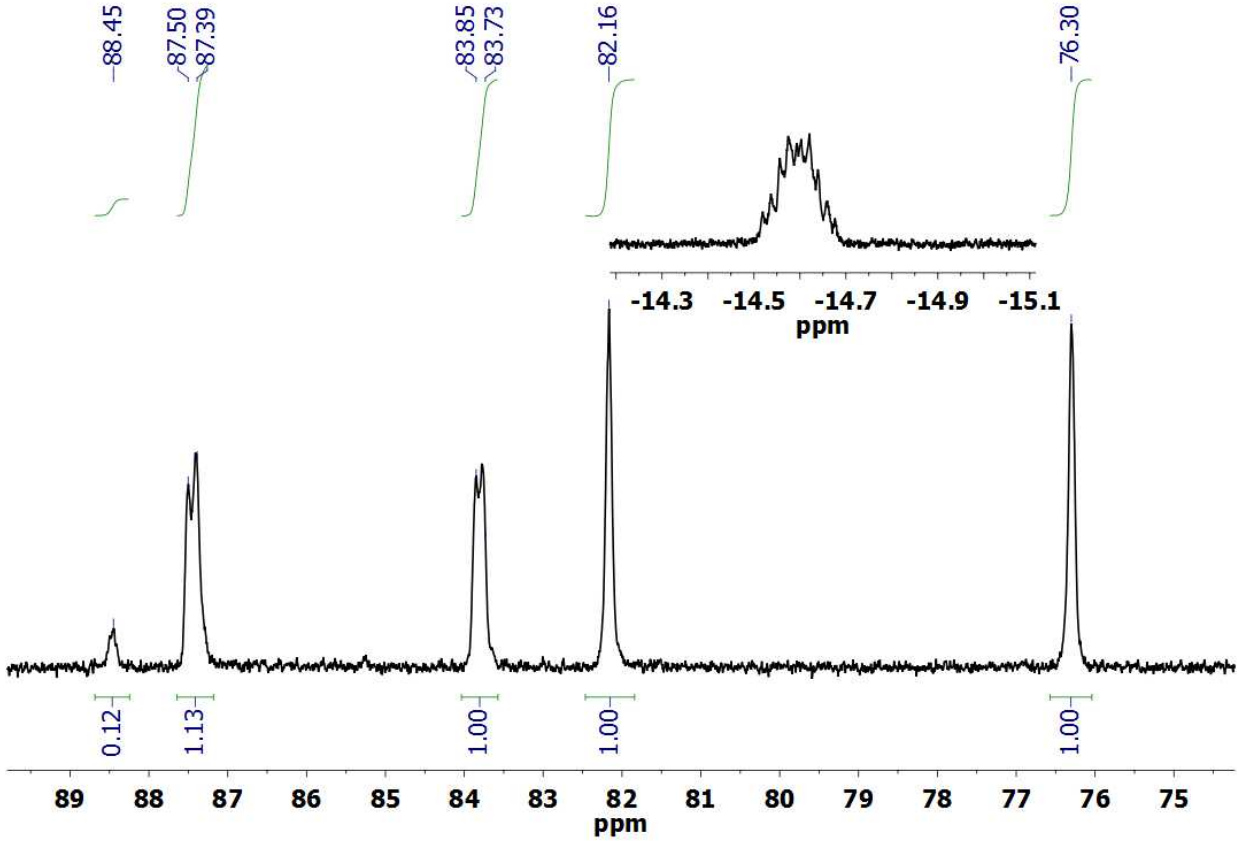

Figure S12. $^{31}P\{^{1}H\}$ NMR spectrum for the reaction of $[H_2Fe_2(pdt)(dppv)_2(CO)]^0$ and $H(Et_2O)_2BAr^F{}_4$ in CH_2Cl_2 solution under ^{13}CO. *Insert:* ^{1}H NMR spectrum in the hydride region.

Assignment:

δ 87.5 (d, $J_{C\text{-}P}$ = 18 Hz), 83.8 (d, $J_{C\text{-}P}$ = 18 Hz), 82.1 and 76.3 = ab-bb isomer.

δ 88.4 (br), and 87.4 (overlapping with δ 87.5 of ab-bb isomer) = ab-ab isomer.

These results and combined with ESI-MS analysis indicate the formation of $[HFe_2(pdt)(dppv)_2(CO)(^{13}CO)]^+$.

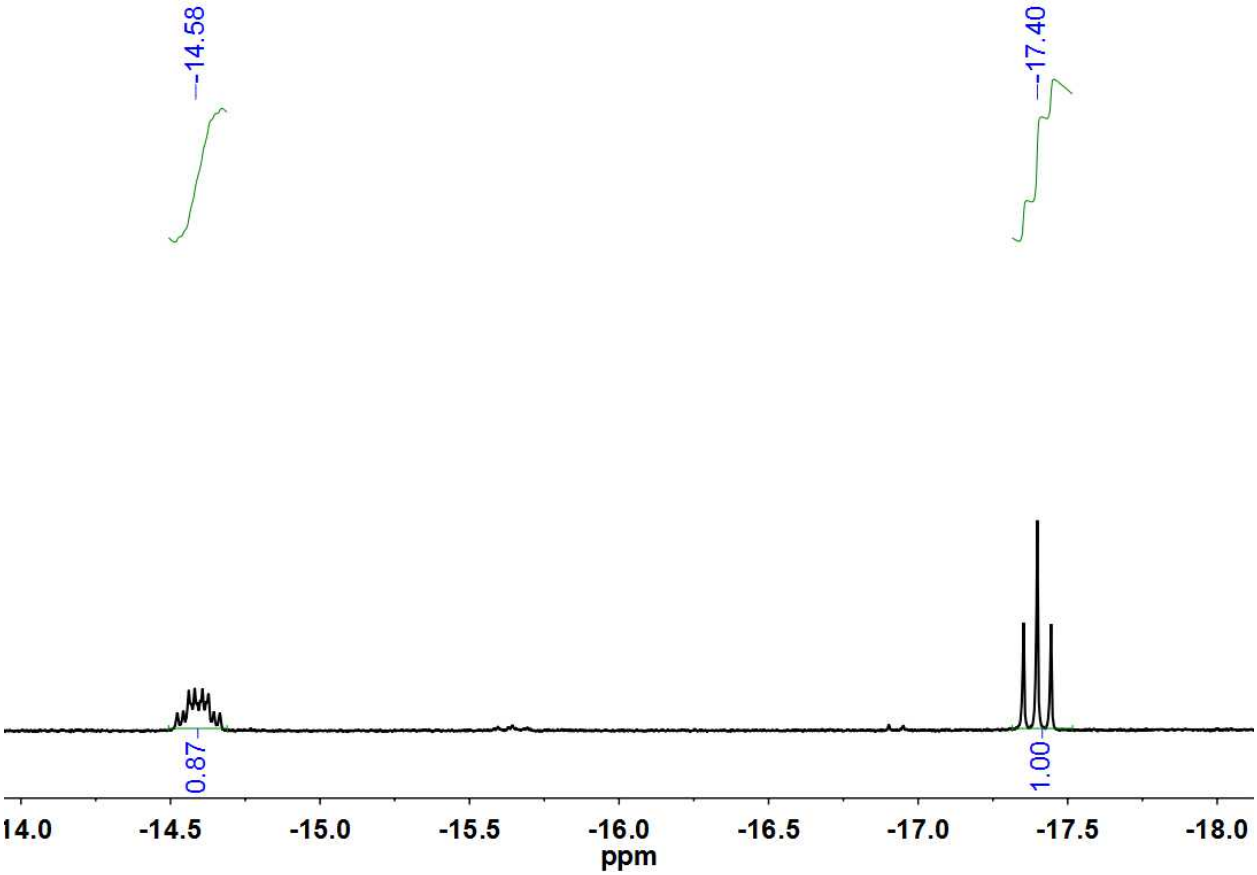

Figure S13. ^{1}H NMR spectrum (hydride region) for the reaction of $[H_2Fe_2(pdt)(CO)(dppv)_2]^0$, $H(Et_2O)_2BAr^F{}_4$, and CO in CD_2Cl_2 solution in the presence of one equiv of integration standard $[HFe_2(edt)(CO)_4(PMe_3)_2]PF_6$ (δ -17.4).

The ratio $[HFe_2(pdt)(CO)_2(dppv)_2]^+$:$[HFe_2(edt)(CO)_4(PMe_3)_2]^+$ = 0.87:1.

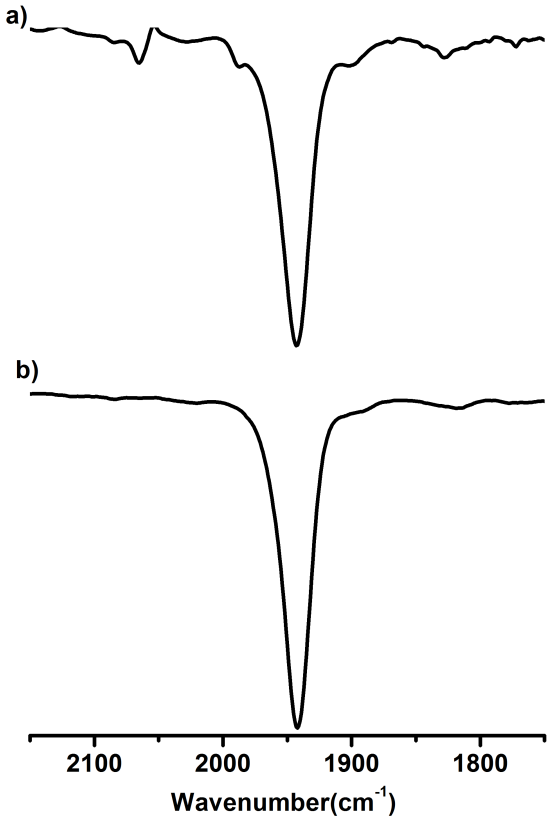

Figure S14. IR spectrum for (a) the reaction of $[H_2Fe_2(pdt)(CO)(dppv)_2]^0$ and $H(Et_2O)_2BAr^F{}_4$ in THF/CH_3CN solution (*v/v* = 95:5); (b) authentic sample of $[HFe_2(pdt)(CO)(NCMe)(dppv)_2]^+$.

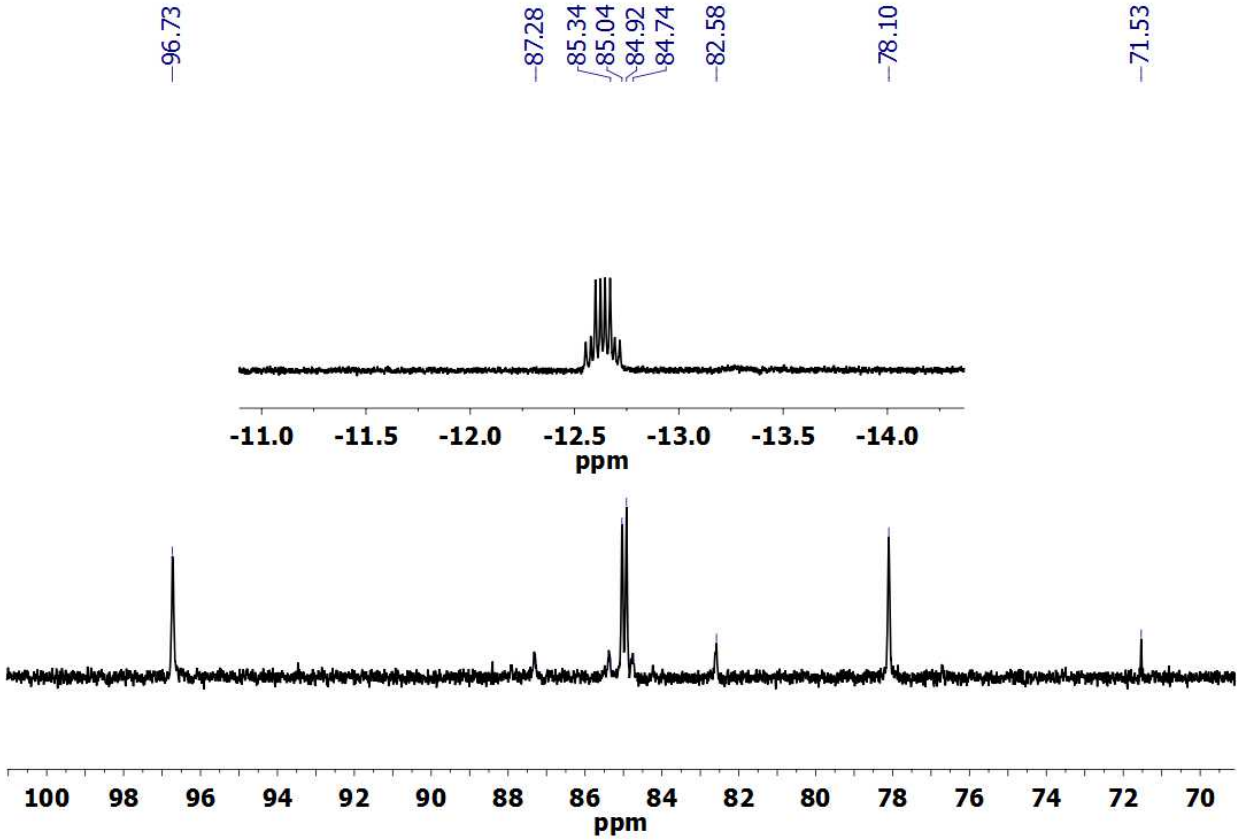

Figure S15. $^{31}P\{^{1}H\}$ NMR spectrum for the reaction of $[H_2Fe_2(pdt)(CO)(dppv)_2]^0$ and $H(Et_2O)_2BAr^F{}_4$ in THF/CH_3CN (*v/v* = 95:5) solution. *Inset:* ^{1}H NMR spectrum of hydride region (μ-H, δ -12.56, m). NMR sample preparation: after reaction the solvent (THF/CH_3CN) was removed, and the residue was re-dissolved in CD_2Cl_2 for NMR analysis.

assignments:
δ 96.7 (s), 85.0 (s), 84.9(s), and 78.1(s) = ab-bb isomer
87.3(s), 85.3(s), 84.7(s) and 82.6 (s) = ab-ab isomer.
δ 71.5 unknown

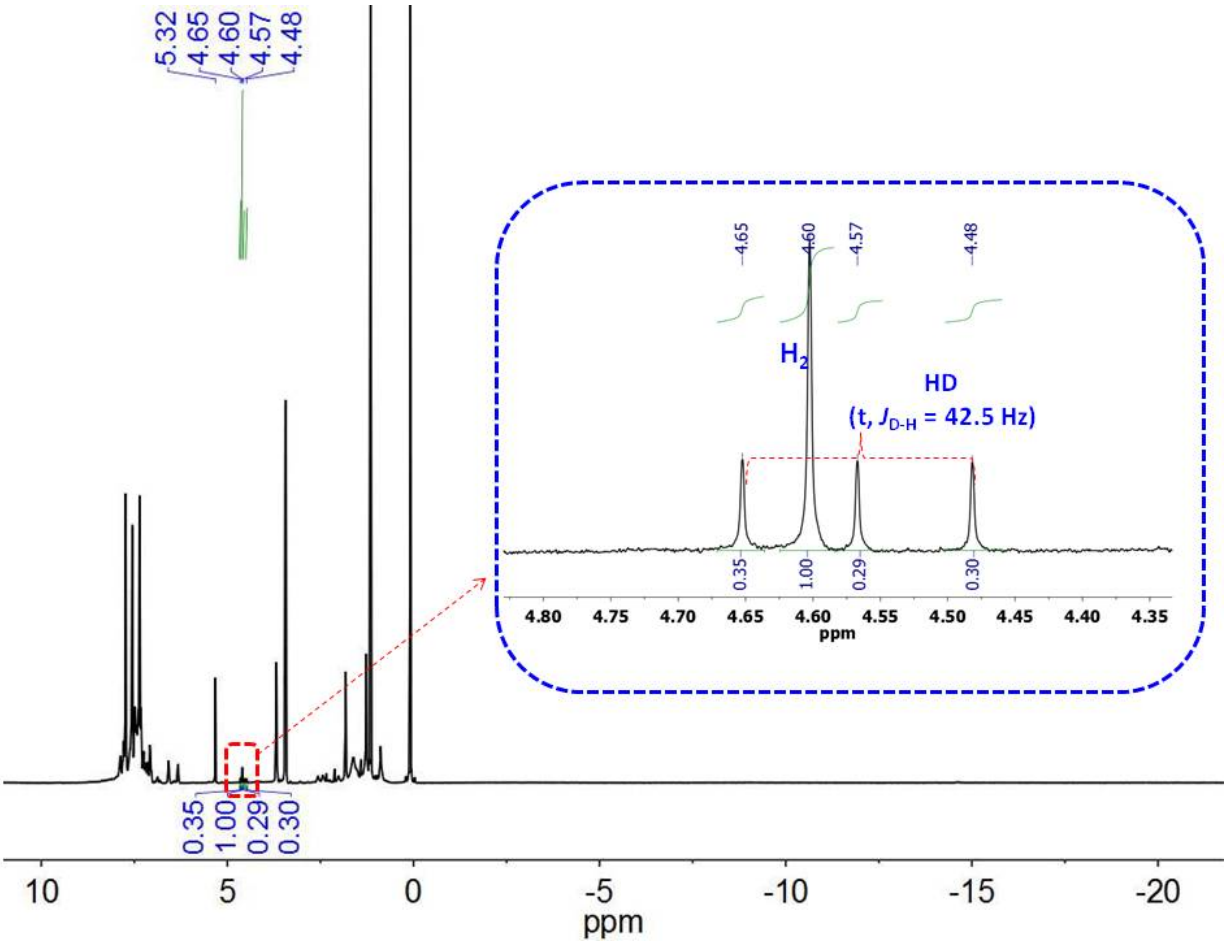

Figure S16. ^{2}H NMR spectrum for the reaction of $[D_2Fe_2(pdt)(CO)(dppv)_2]^0$, $H(Et_2O)_2BAr^F{}_4$, and CO in CD_2Cl_2 solution.

Results： Protonolysis of $[D\mathbf{1}D]^0$ under CO in a sealed NMR tube, a difficult experiment, afforded HD and H_2 in a 2:1 molar ratio.

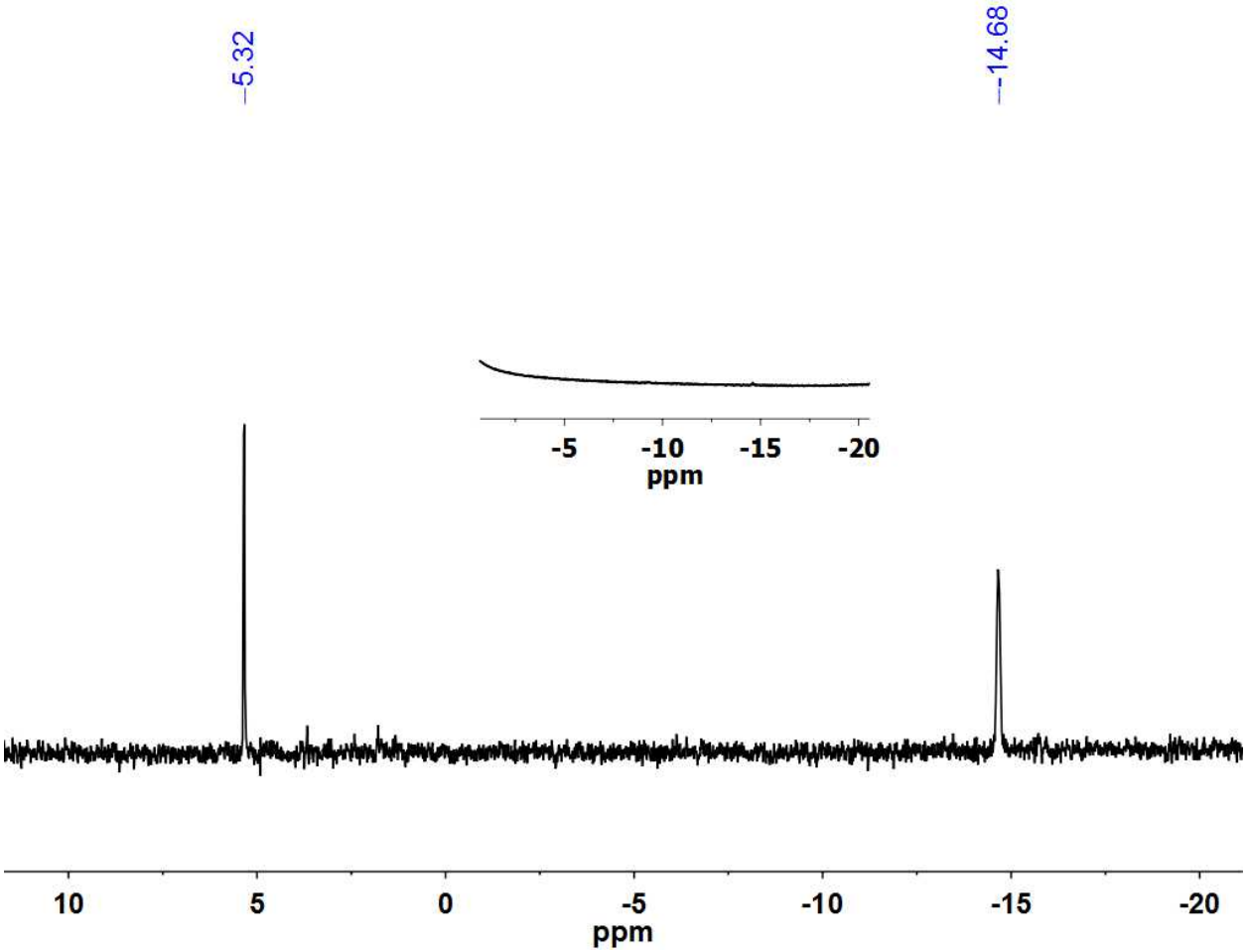

Figure S17. ^{2}H NMR spectrum for the reaction of $[D_2Fe_2(pdt)(CO)(dppv)_2]^0$, $H(Et_2O)_2BAr^F{}_4$, and CO in CH_2Cl_2 solution. Insert: ^{1}H NMR spectrum (hydride region) of the reaction mixture.

Results:

δ -14.68, μ-D of $[DFe_2(pdt)(CO)_2(dppv)_2]^+$

The experiments shows $[DFe_2(pdt)(CO)_2(dppv)_2]^+$ was produced.

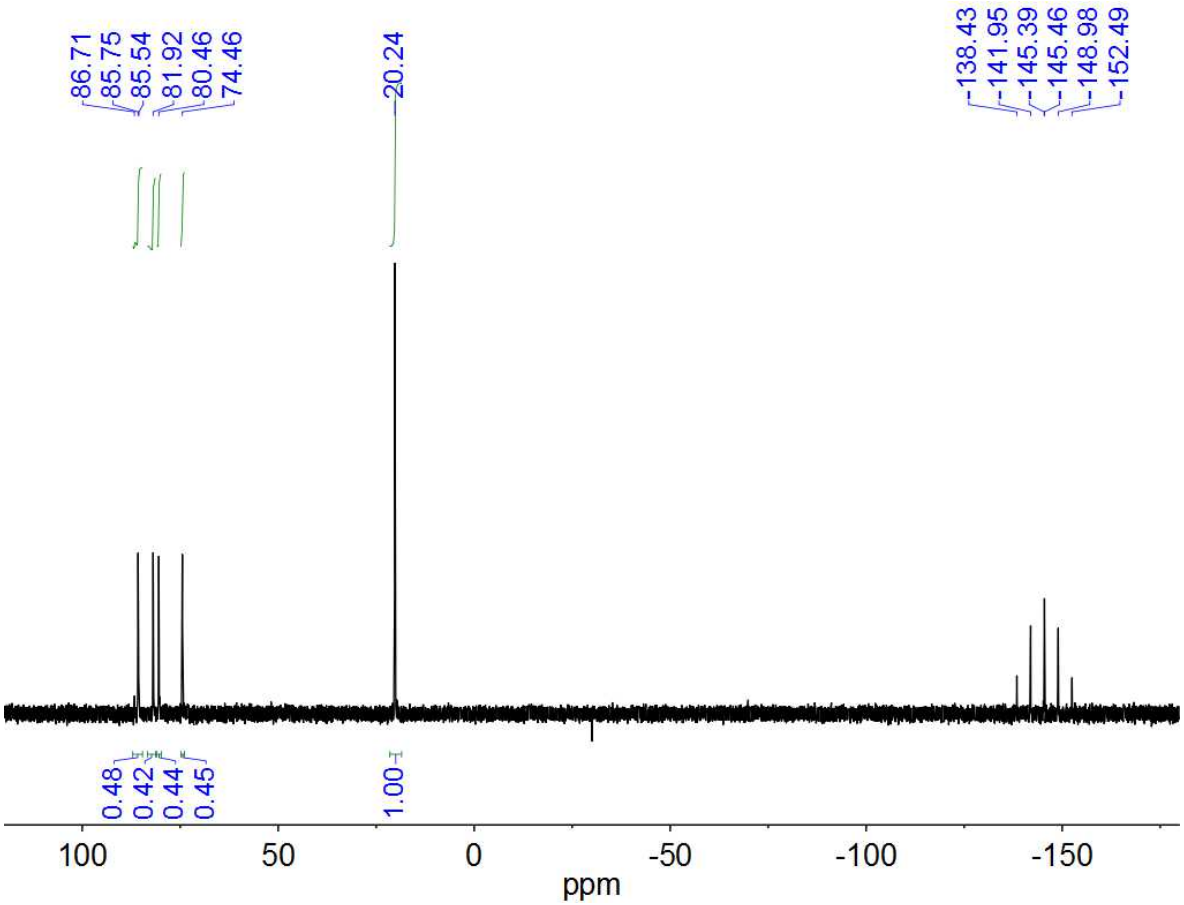

Figure S18. ^{31}P NMR spectrum for the reaction of $[D_2Fe_2(pdt)(CO)(dppv)_2]^0$, $H(Et_2O)_2BAr^F{}_4$, and CO in CH_2Cl_2 solution in. After reaction, 1 equiv of $[HFe_2(edt)(CO)_4(PMe_3)_2]PF_6$ was added as an integration standard.

Assignments: sym-[D**1**(CO)]$^+$: δ 86.71, 85.54; *unsym*-[D**1**(CO)]$^+$: δ 85.75, 81.92, 80.46 and 74.46;
$[HFe_2(edt)(CO)_4(PMe_3)_2]PF_6$: δ 20.24; PF_6^-: δ -149.39 (septet).

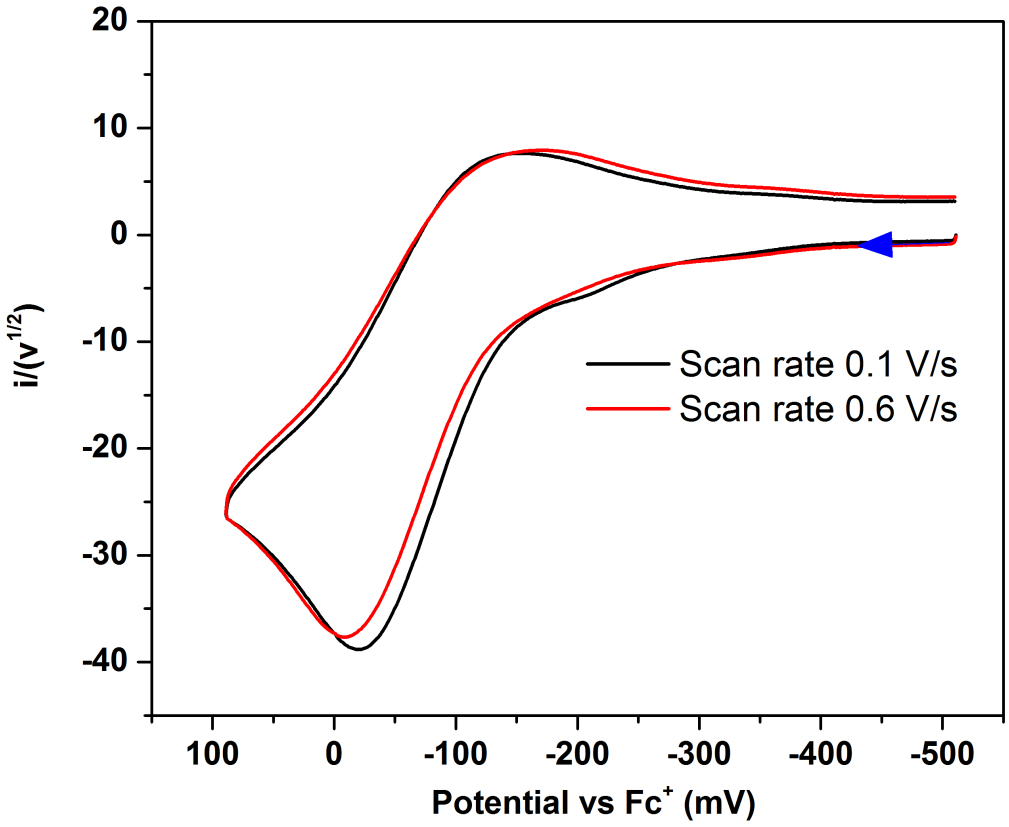

Figure S19. Cyclic voltammogram of $[H_2Fe_2(pdt)(CO)(dppv)_2]^0$ ($[H\mathbf{1}H]^0$) in THF solution. *Conditions:* 1.0 mM $[H\mathbf{1}H]^0$, 100 mM $[Bu_4N]PF_6$ in, 25 °C, 0.1 and 0.6 V/s scan rate, referenced to $Fc^{+/0}$.

Results: $E_{1/2}[H\mathbf{1}H]^{0/+}$ = -70 mV. The reversibility of this oxidation event was not increased at a higher scan rate of 0.6 V/s (or higher to 1 V/s).

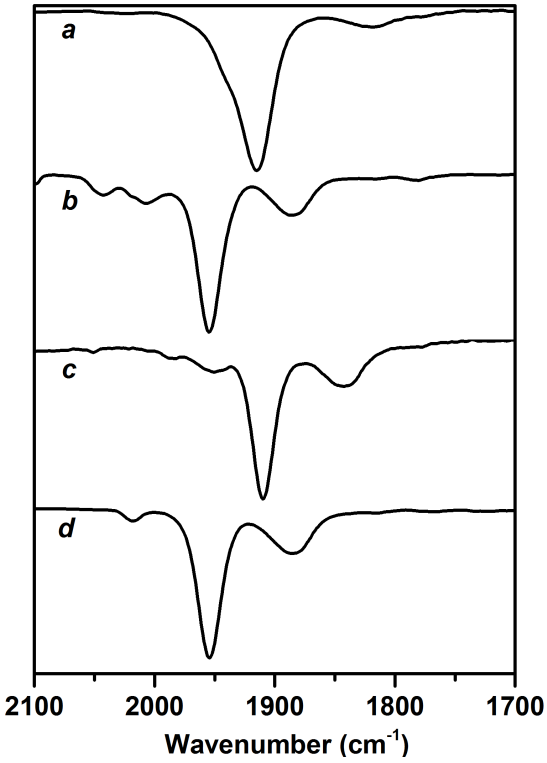

Figure S20. IR spectra (ν_{CO} region) of (a) $[H_2Fe_2(pdt)(CO)(dppv)_2]^0$ ($[H\mathbf{1}H]^0$; (b) for the reaction of $[H\mathbf{1}H]^0$, $FcBAr^F_4$ and CO; (c) (b) for the reaction of $[H\mathbf{1}H]^0$, $FcBAr^F_4$ and ^{13}CO; (d) $[Fe_2(pdt)(CO)_2(dppv)_2]BAr^F_4$ in THF solution.

Results: a) ν_{CO} (cm^{-1}, THF), 1915.

b) ν_{CO} (cm^{-1}, THF), 1955, 1884.

c) ν_{CO} (cm^{-1}, THF), 1910, 1843.

d) ν_{CO} (cm^{-1}, THF), 1955, 1884.

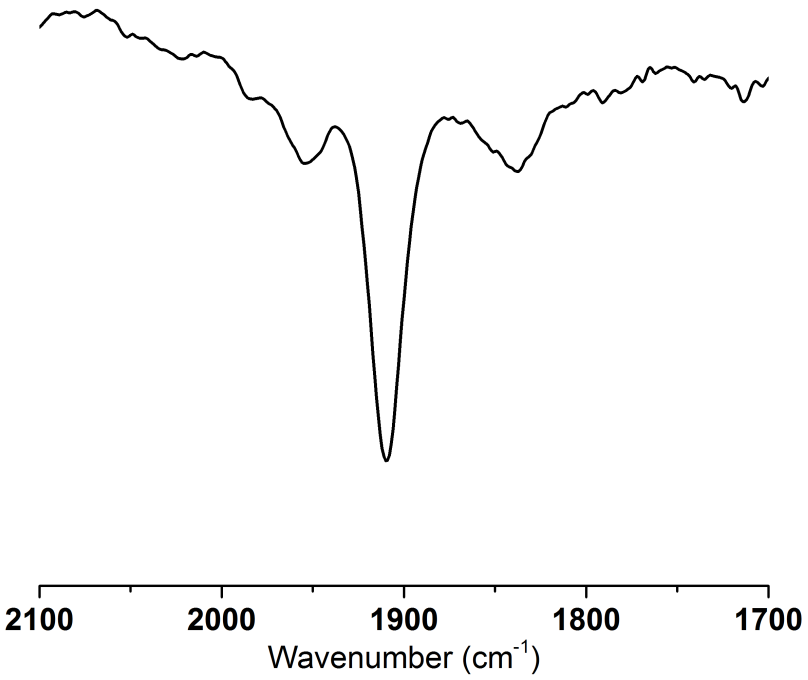

Figure S21. IR spectrum for the reaction mixture of $[Fe_2(pdt)(CO)_2(dppv)_2]BAr^F{}_4$ and ^{13}CO in THF solution for 2 h at RT.

Results: ν_{CO} (cm^{-1}, THF), 1910, 1843, which shows the same as the spectrum in Figure S13 c.

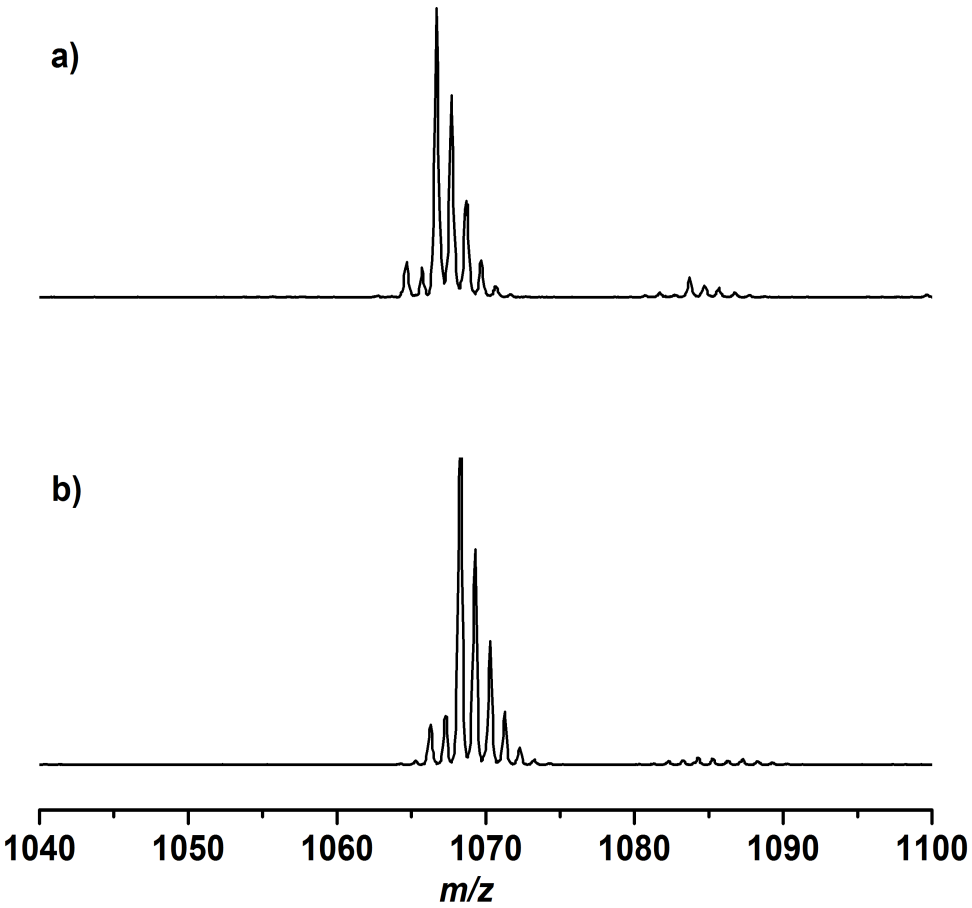

Figure S22. ESI-MS mass spectrum for the reaction mixture of $[H\mathbf{1}H]^0$, $FcBAr^F{}_4$ under CO (a) and ^{13}CO (b) atmosphere in THF solution.

Results: (a) ESI-MS, *m/z* = 1066.7

(b) ESI-MS, *m/z* = 1068.4.

Combining with the results in Figure S13, 14 and GC analysis for H_2 production, the following reactions were observed:

1) $[H_2Fe_2(pdt)(dppv)_2(CO)]^0 - e + CO \rightarrow [Fe_2(pdt)(dppv)_2(CO)_2]^+ + H_2$
2) $[H_2Fe_2(pdt)(dppv)_2(CO)]^0 - e + {}^{13}CO \rightarrow [Fe_2(pdt)(dppv)_2(CO)({}^{13}CO)]^+ + H_2$
   $[Fe_2(pdt)(dppv)_2(CO)({}^{13}CO)]^+ + {}^{13}CO \rightarrow [Fe_2(pdt)(dppv)_2({}^{13}CO)_2]^+ + CO$

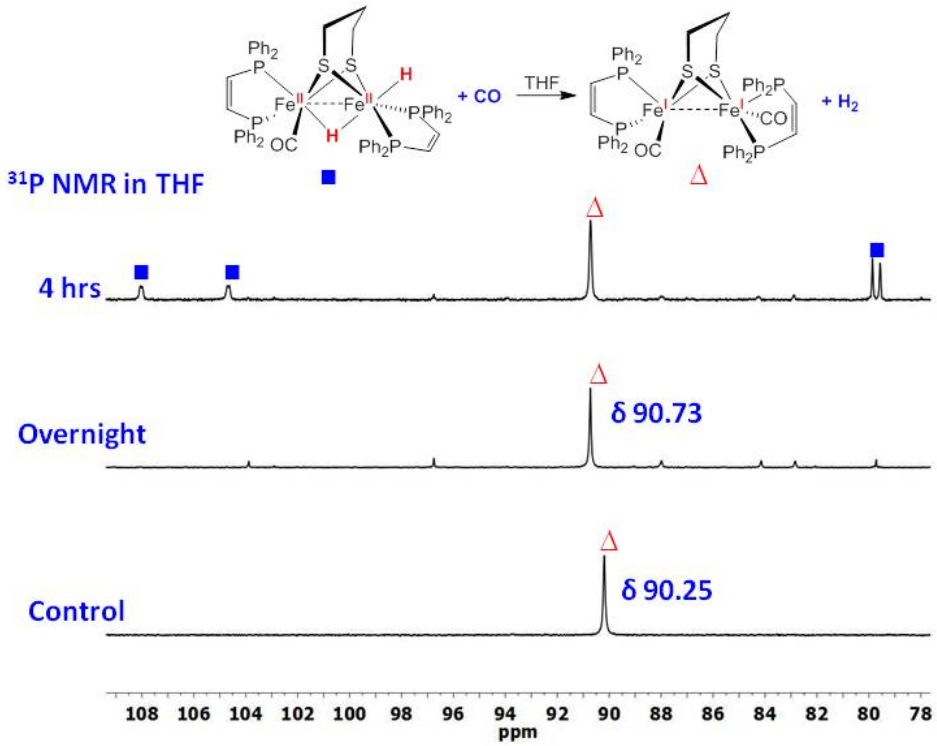

Figure S23. $^{31}P\{^{1}H\}$ NMR spectra for the reaction of $[H\mathbf{1}H]^0$ and CO in THF solution after 4 h (*top*), overnight (*middle*) and the control $Fe_2(pdt)(CO)_2(dppv)_2$ (**1**(CO)) for (*bottom*).

Assignment:

Top, δ 108, 105, 80 and 78 for $[H\mathbf{1}H]^0$, a new peak at δ 90.7 for **1**(CO) was observed.

Middle, $[H\mathbf{1}H]^0$ is absent at this stage. δ 90.7 is assigned to **1**(CO) together with small amounts of unidentified contaminents.

Bottom, δ 90.7 for **1**(CO).

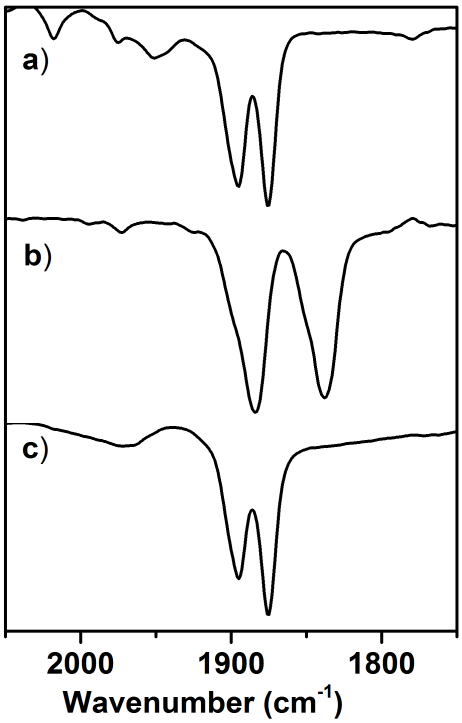

Figure S24. IR spectra of THF solution of $[H\mathbf{1}H]^0$ under CO (a) ^{13}CO (b) atmospheres for 12 h at room temperature. Spectrum (c) corresponds to authentic $Fe_2(pdt)(CO)_2(dppv)_2$.

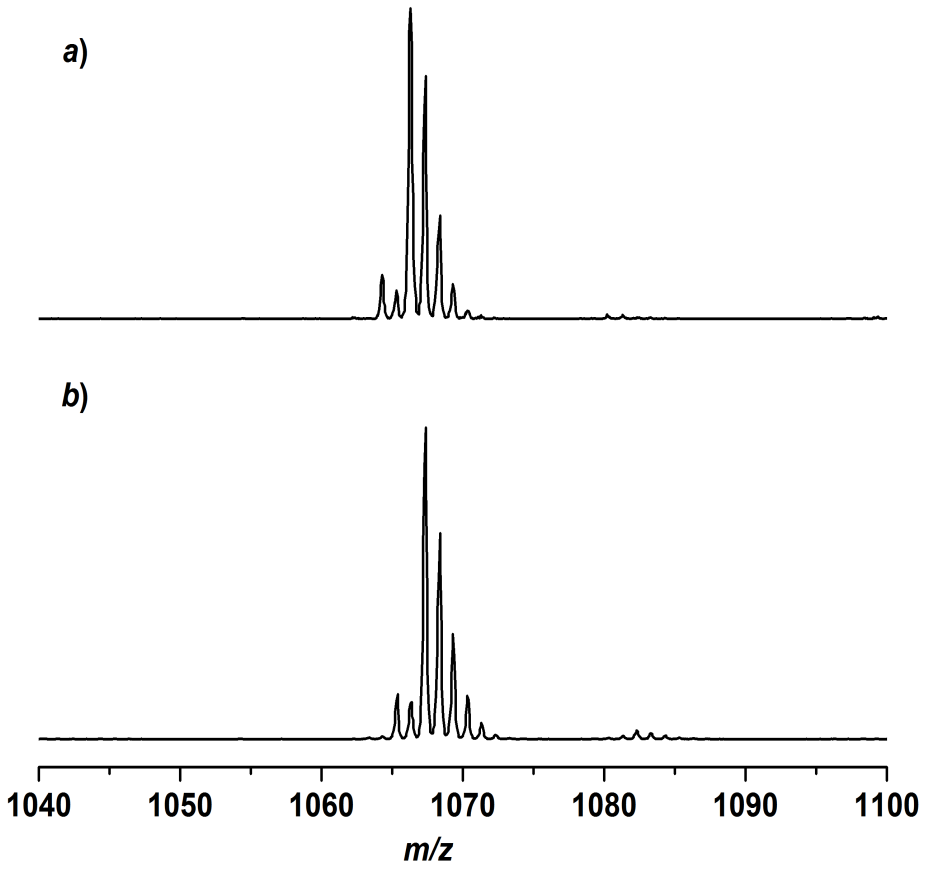

Figure S25. ESI-MS mass spectrum for the reaction mixture of $[H\mathbf{1}H]^0$ and CO (a) and ^{13}CO (b) in THF solution.

Results: Mass spectrum, ^{31}P NMR and IR analysis indicate the following reaction,

$$[H_2Fe_2(pdt)(dppv)_2(CO)]^0 + {}^{13}CO \rightarrow [Fe_2(pdt)(dppv)_2(CO)({}^{13}CO)] + H_2.$$

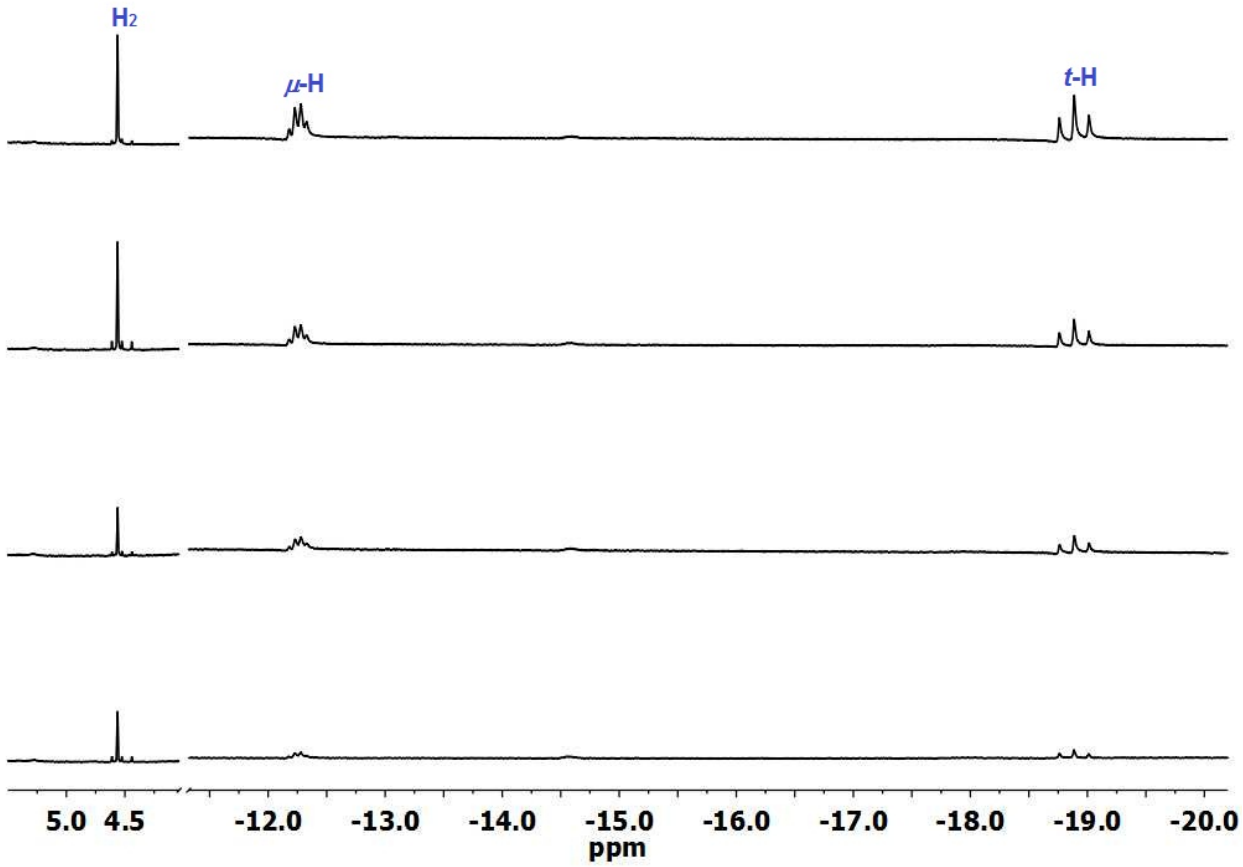

Figure S26. ^{1}H NMR spectrum for the reaction of [H**1**H]^{0} and D_2 in THF-d_8 solution at -40 ºC for 2, 4, 6, and 8 h (from top to bottom).

Results: H_2 produced from the reaction was observed at δ 4.57 (s) together with small amount of HD (~10%); the intensities of two hydride signals at δ -12.24 and -18.90 decrease.

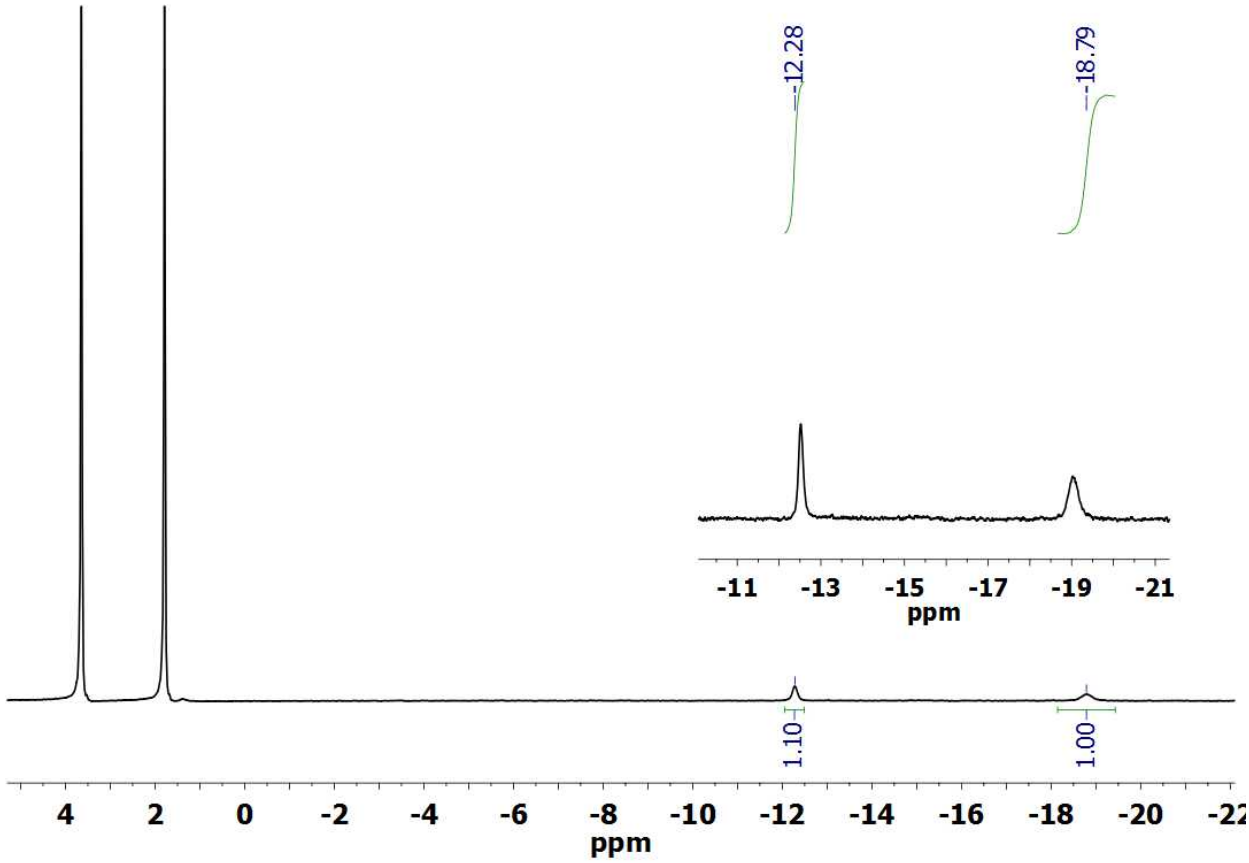

Figure S27. ^{2}H NMR spectrum for [D**1**D]^{0} in THF/THF-d_8 (v/v = 95/5) solution at -40 ºC.

Results: μ-D, δ -12.28; *t*-D, -18.79.

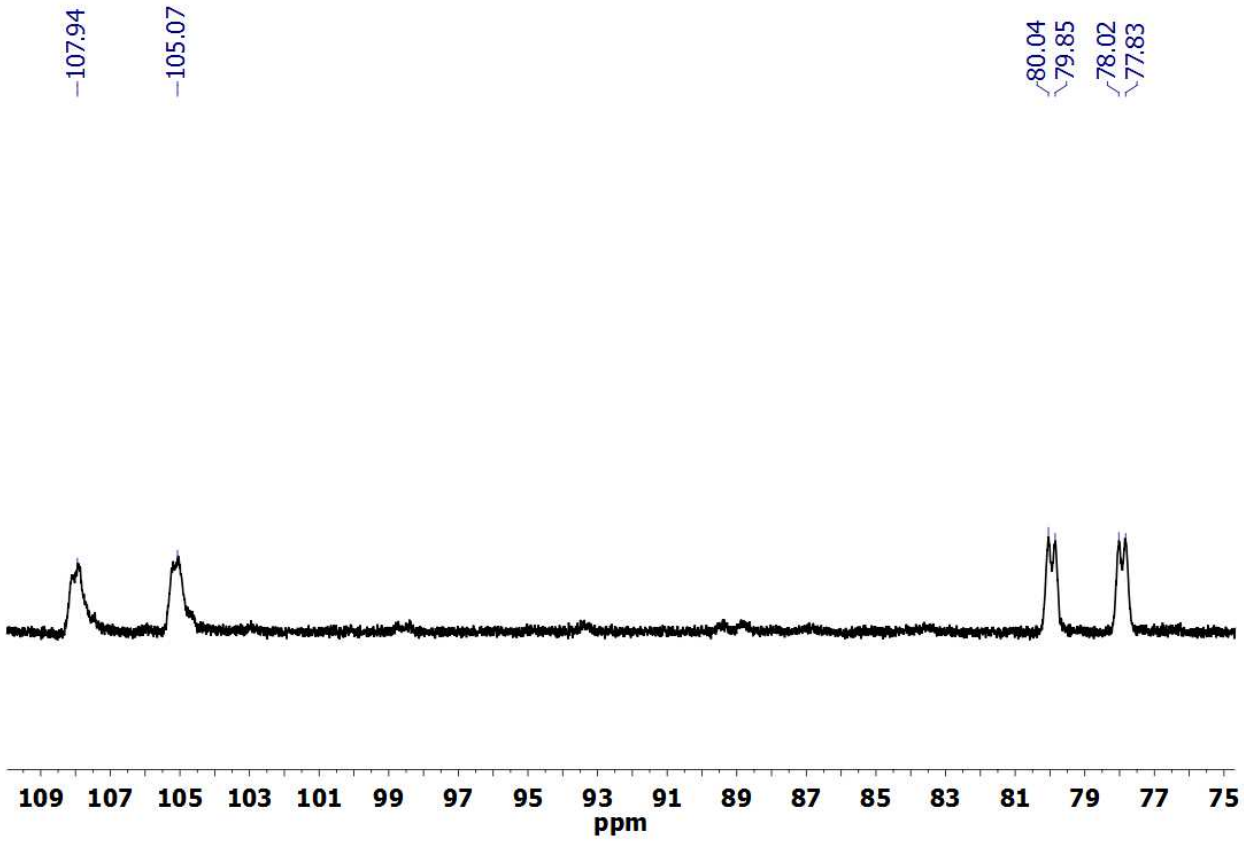

Figure S28. $^{31}P\{^{1}H\}$ NMR spectrum for isolated [D**1**D]^{0} in THF solution at -40 ºC. *Assignments:* [D1D]^{0}, δ 107.9 (br), 105.1 (br), 80 (d), 78(d).

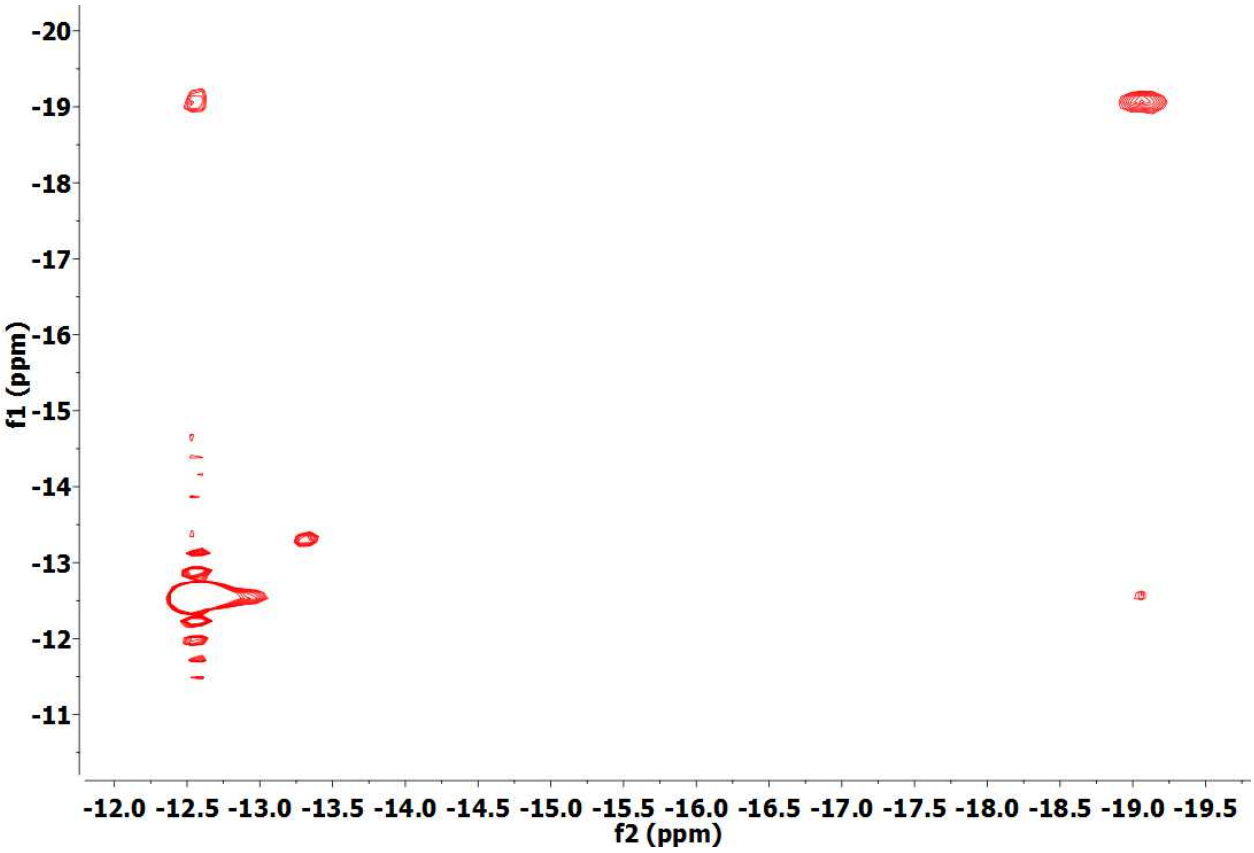

Figure 29. (^{2}H,^{2}H) EXSY spectrum (hydride region) of [D**1**D]^0 in THF-d_8 solution at -40 ºC with a mixing time of 500 ms.

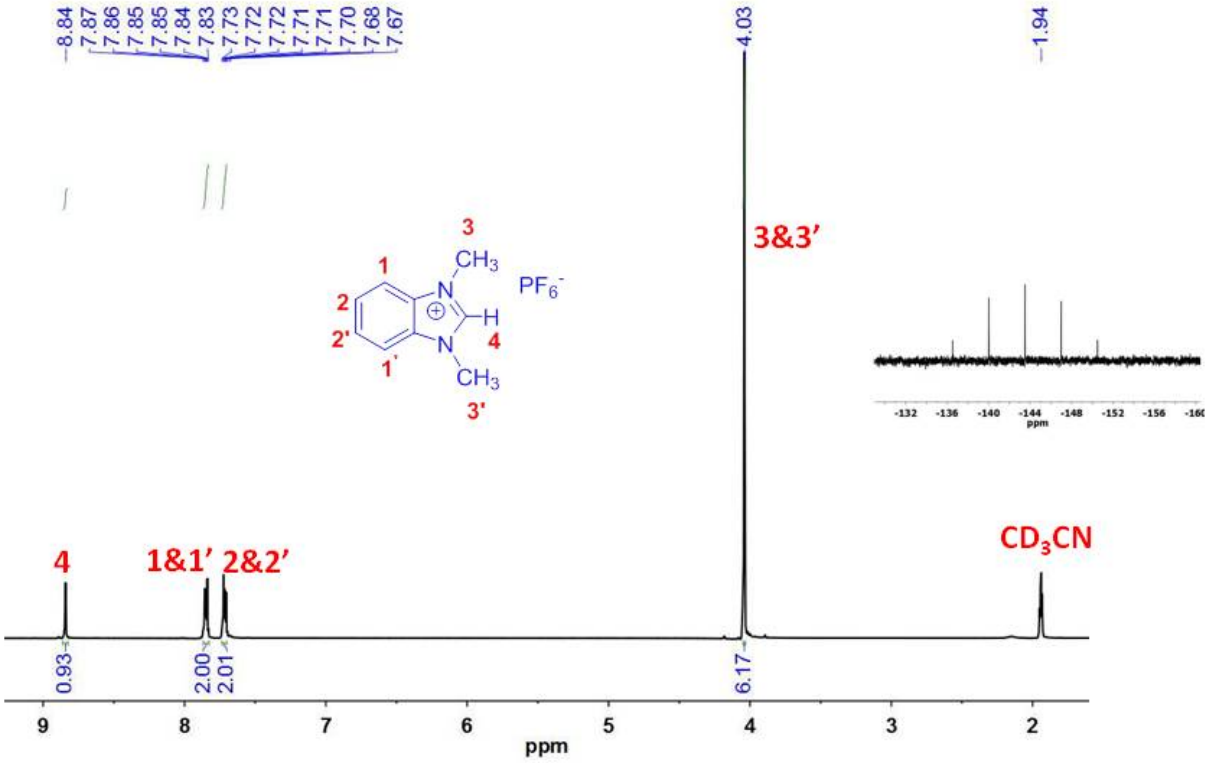

Figure S30. ^{1}H NMR (in CD_3CN) of 1,3-dimethylbenzimidazolium hexafluorophosphate. Insert: ^{31}P signals of PF_6^- anion.

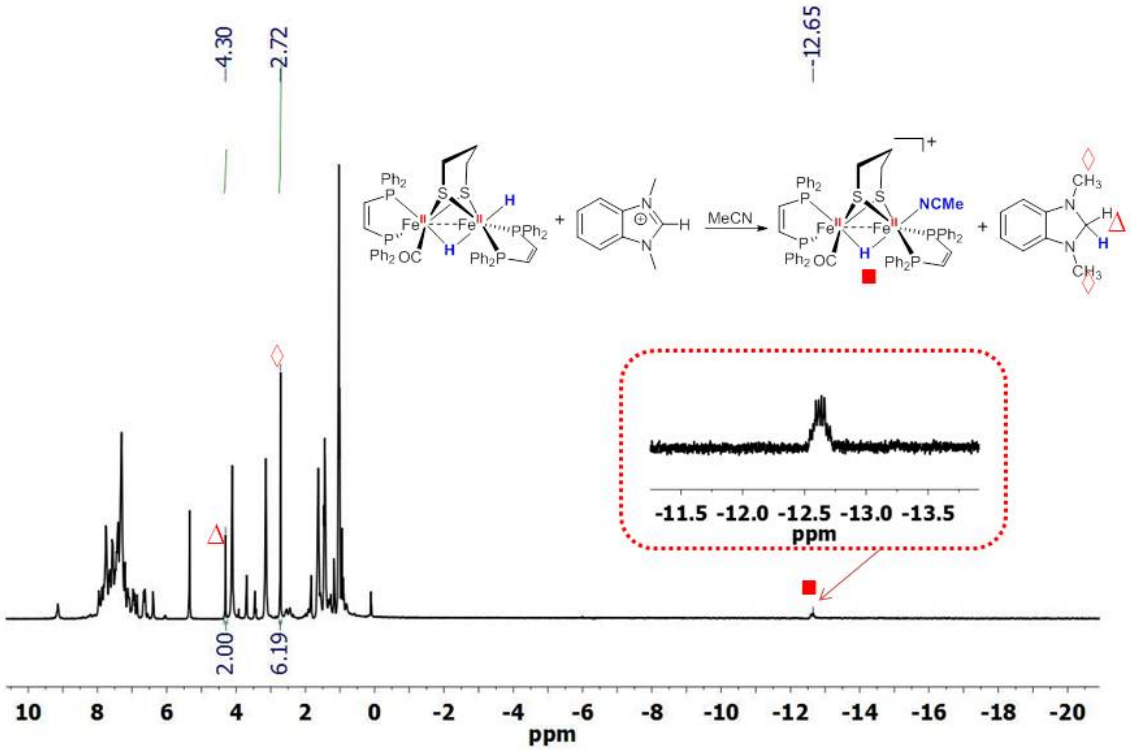

Figure S31. ^{1}H NMR spectrum for the reaction mixture of [H**1**H]^{0} and 1,3-dimethylbenzimidazolium in CD_3CN at room temperature.

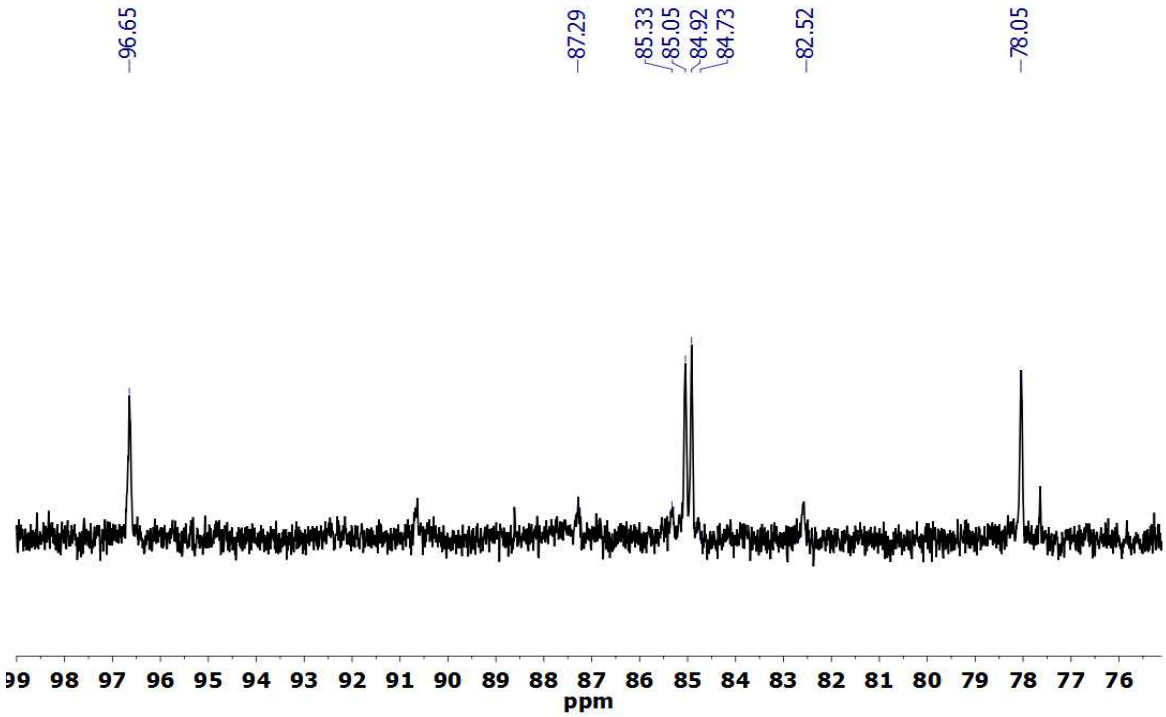

Figure S32. $^{31}P\{^{1}H\}$ NMR spectrum for the reaction mixture of $[H\mathbf{1}H]^{0}$ and 1,3-dimethylbenzimidazolium in CD_3CN at room temperature.
Assignments: The ^{31}P combined with ^{1}H NMR spectrum indicate the formation of $[HFe_2(pdt)(dppv)_2(CO)(NCMe)]^{+}$; ab-bb isomer, δ 96.6 (s), 85 (s), 84.9 (s) and 78 (s); ab-ab isomer, δ 87.3 (s), 85.3 (s), 84.7 (s) and 82.5 (s).

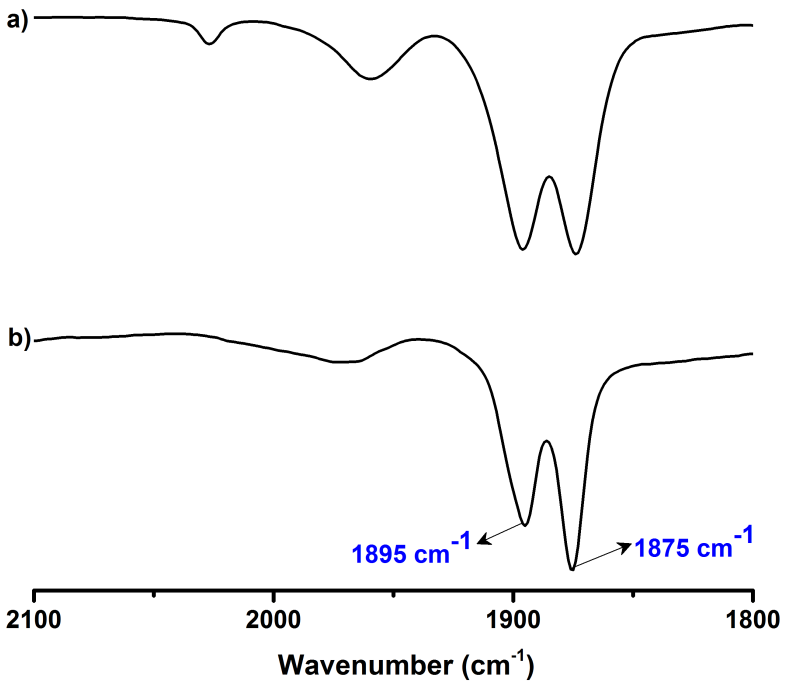

Figure S33. IR spectrum for (a) the reaction of $[H\mathbf{1}H]^0$ and Dimethyl acetylenedicarboxylate (DMDA) under CO. Spectrum (c) corresponds to authentic $Fe_2(pdt)(CO)_2(dppv)_2$ in CH_2Cl_2.

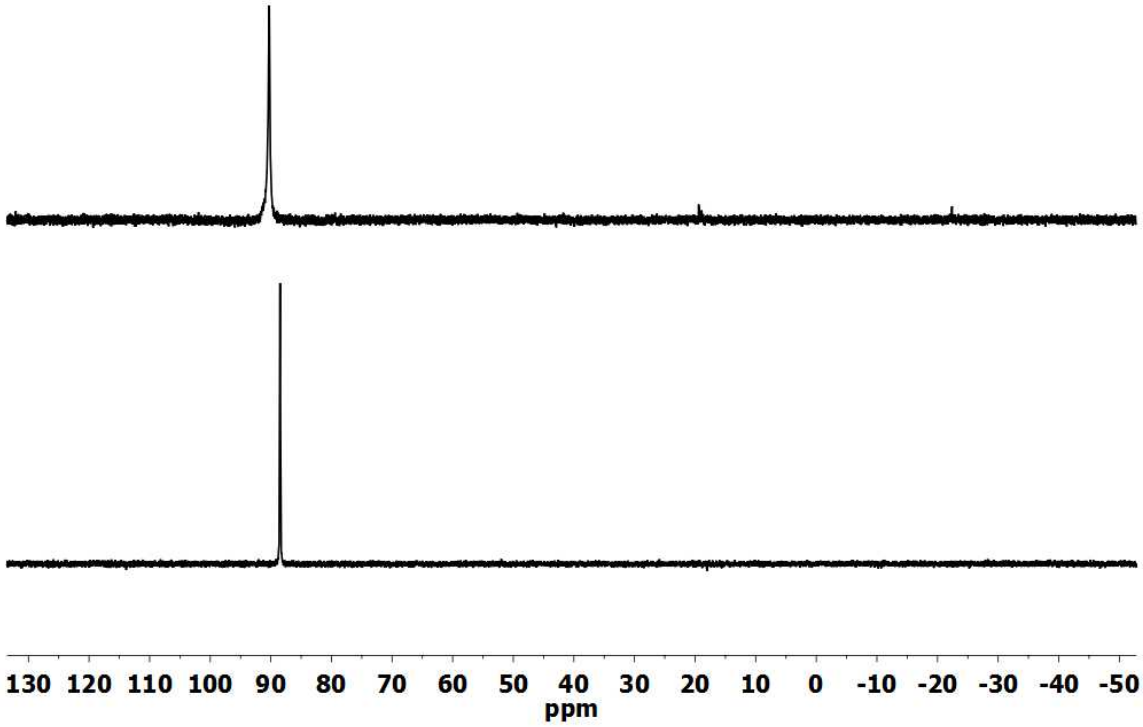

Figure S34. ^{31}P NMR (CH_2Cl_2) spectra for the reaction of [H**1**H]^0 and DMDA under CO (*top*), and (*bottom*) for authentic $Fe_2(pdt)(CO)_2(dppv)_2$

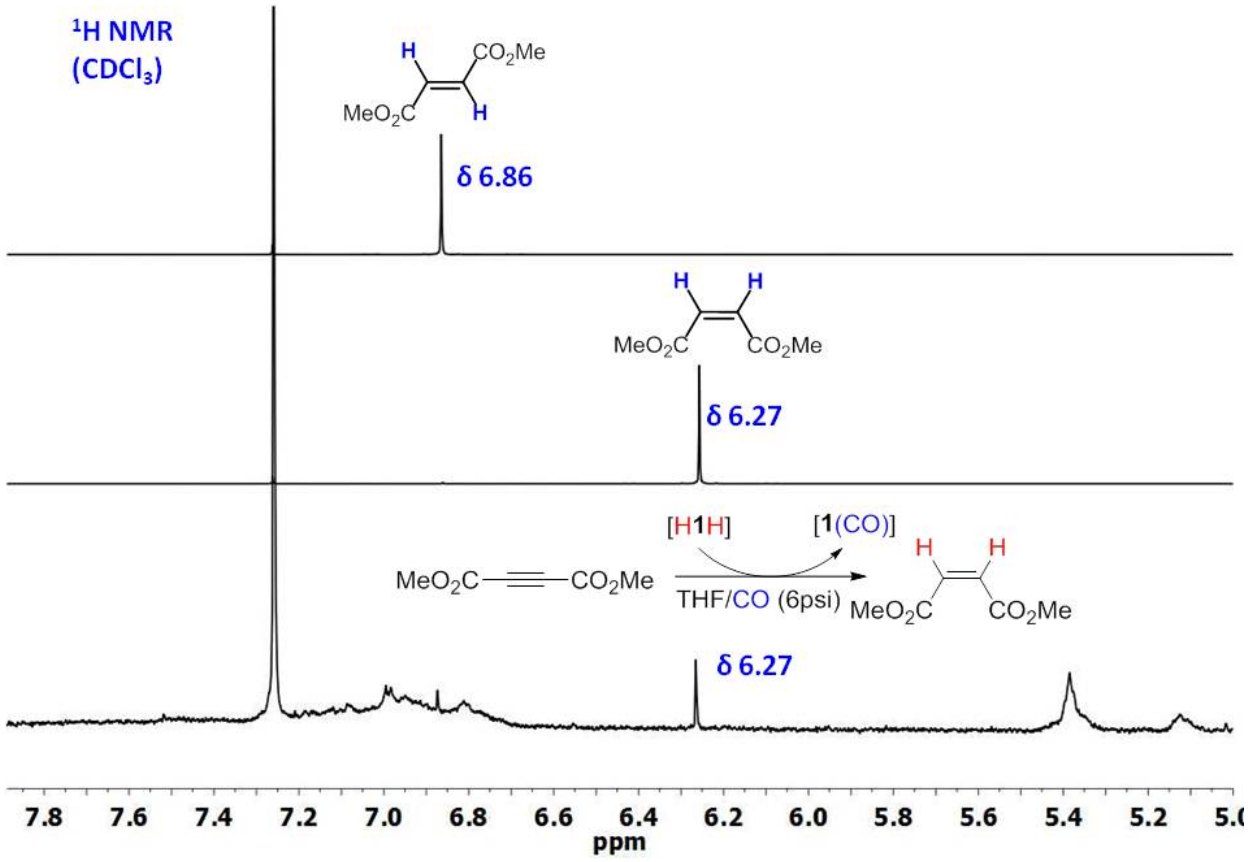

Figure S35. ^{1}H NMR ($CDCl_3$) spectra of *trans*-MeO_2CCH=$CHCO_2Me$ (*top*), *cis*-MeO_2CCH=$CHCO_2Me$ (*middle*), and (*bottom*) for the organic product extracted from the reaction of [H**1**H]^0 and DMDA under CO.

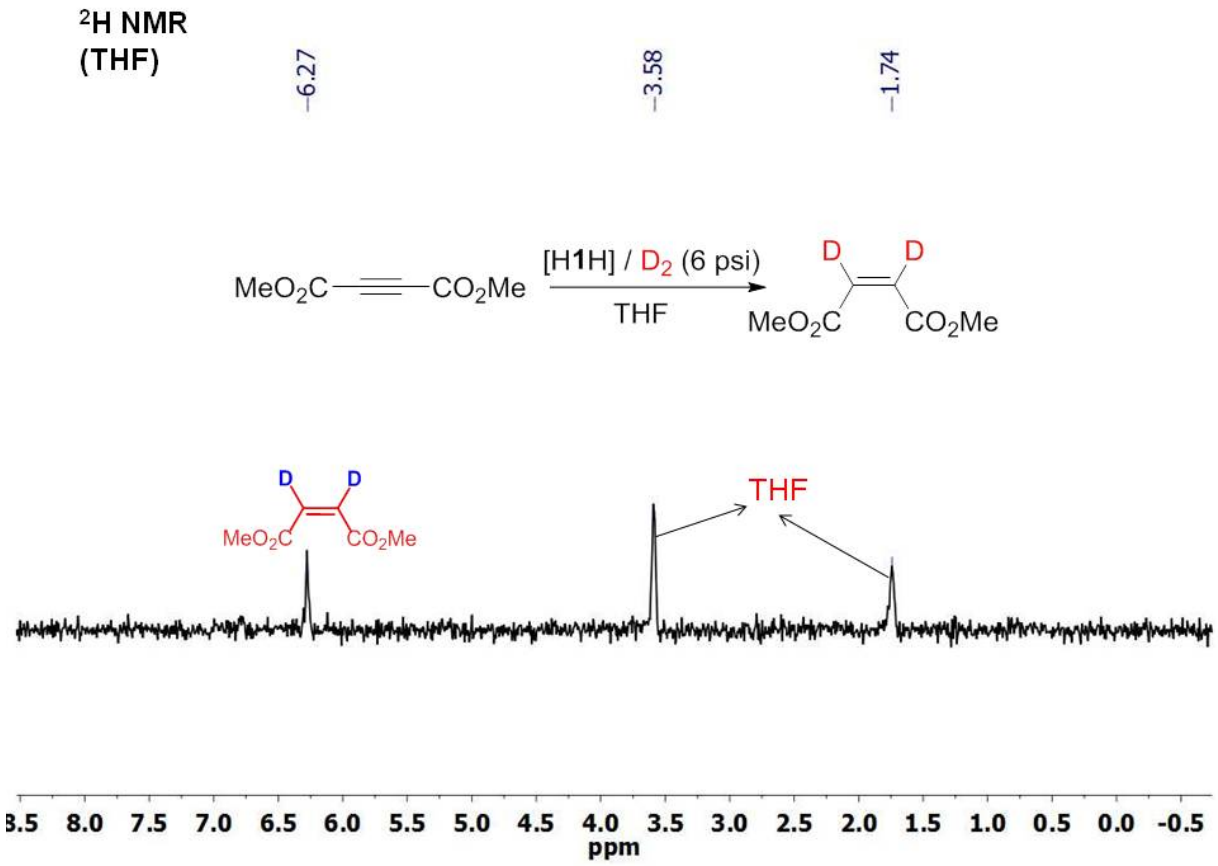

Figure S36. ^{2}H NMR (THF) spectrum for *cis*-MeO_2CCD=$CDCO_2Me$ isolated from the reaction of $[H\mathbf{1}H]^0$ and DMDA under D_2.

Results: Combined with Figures S33-36, The results suggests that from the reaction of $[H\mathbf{1}H]^0$ and DMDA under CO produces [**1(CO)**] and *cis*-MeO_2CCH=$CHCO_2Me$.

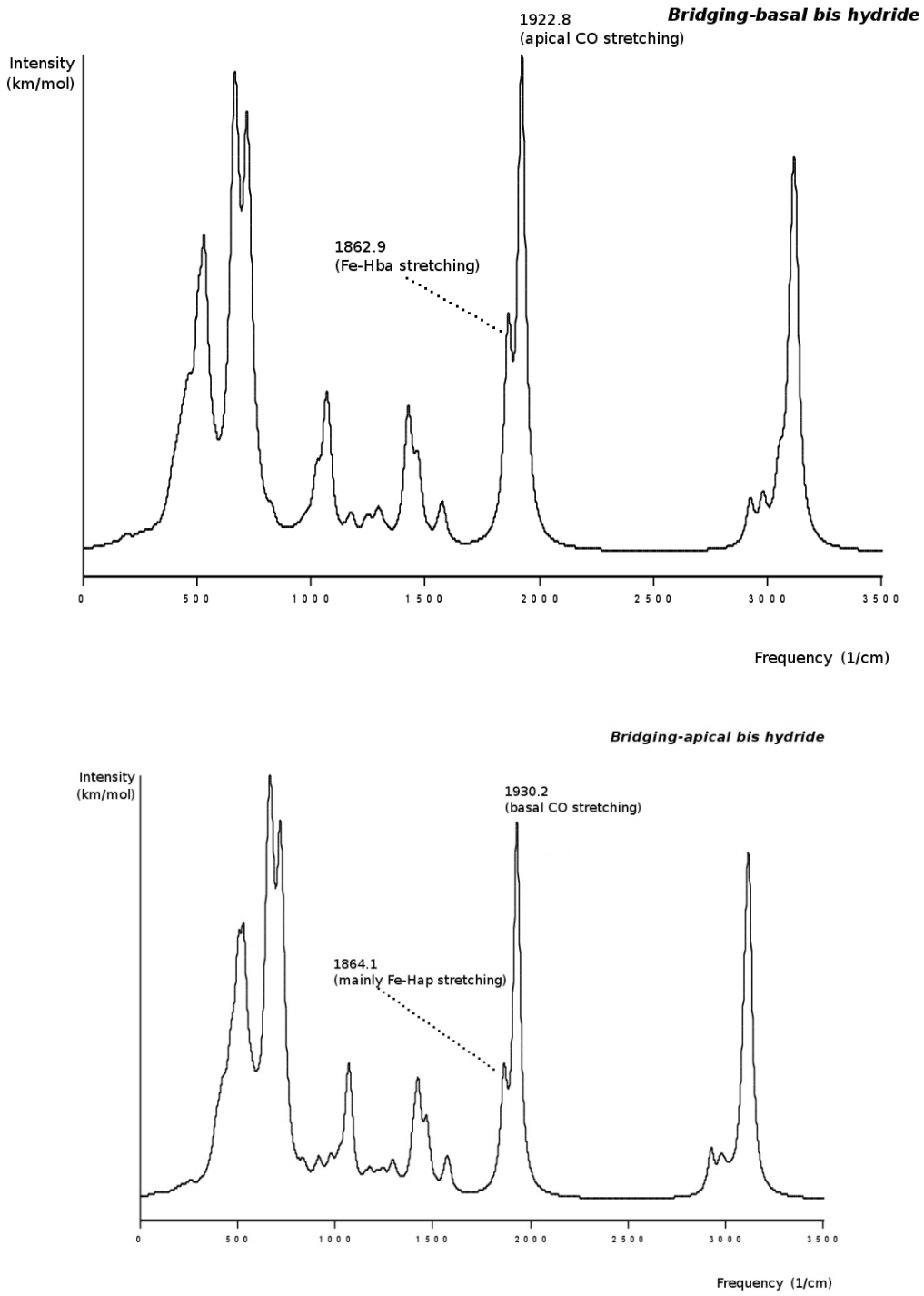

Figure S37. DFT-calculated IR spectra (ν_{CO} region) of two isomers of $[H_2Fe_2(pdt)(CO)(dppv)_2]^0$.

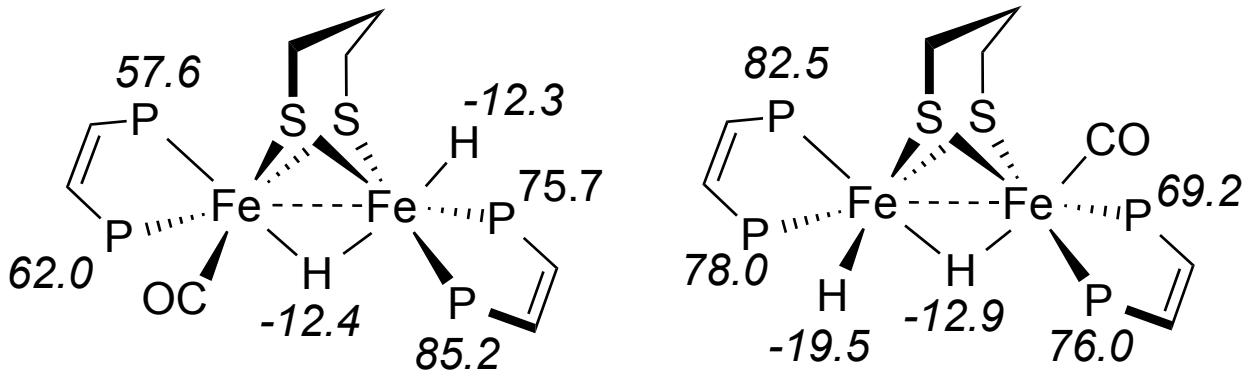

Figure S38. DFT-calculated ^{1}H and ^{31}P NMR spectra for two isomers of $[H_2Fe_2(pdt)(CO)\text{-}(Me_2PCH{=}CHPMe_2)_2]^0$ (ppm, vs TMS and H_3PO_4).

Table S1. Calculated geometry for ground state for $[H\mathbf{1}H]^0$. Selected parameters for transition state/intermediate (shown in next figure) in H-H exchange are shown in parentheses.

Structural Parameter	***Value (Å or deg)***
Fe1-Fe2	2.660 (2.648)
Fe1-H1	1.673 (1.551)
Fe1-H2	1.527 (1.558)
Fe1-P1	2.175 (2.191)
Fe1-P2	2.200 (2.211)
Fe1-S1	2.270 (2.250)
Fe1-S2	2.255 (2.274)
Fe2-C	1.748 (1.745)
Fe2-H1	1.750 (2.496)
Fe2-P3	2.248
Fe2-P4	2.251
Fe2-S1	2.321
Fe2-S2	2.286
H2-Fe1-H1	79.6
H2-Fe1-Fe2	107.2
H2-Fe1-P1	83.0 (89.1)
H2-Fe1-P2	86.6 (96.7)
H2-Fe1-S1	161.7 (145.0)
H2-Fe1-S2	88.3 (85.0)
H1-Fe1-P1	162.6 (125.1)
H1-Fe1-S1	82.5
H1-Fe1-S2	81.2 (92.1)
P1-Fe1-S1	114.8
P2-Fe1-S2	172.0
H1-Fe2-C	175.9
H1-Fe2-S1	79.4 (110.0)
H1-Fe2-S2	78.9
H1-Fe2-P3	90.4
C-Fe2-S1	97.2
C-Fe2-P3	87.7
S1-Fe2-P4	171.9
P1-Fe1-Fe2-C	31.6

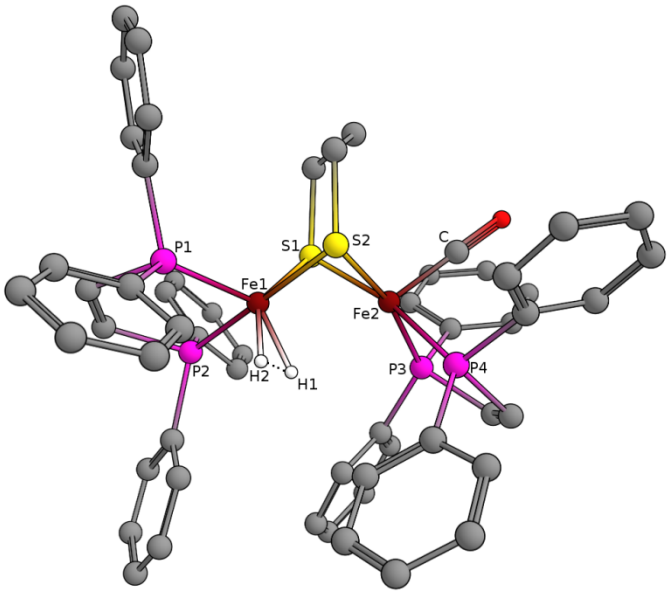

Table S2. Calculated IR frequencies.

[H1H]^0 Species	***DFT/BP86/TZVP IR (CO stretching region; cm^{-1})***
Basal-bridging HH; (a-b)(b-b) $(dppv)_2$	1923; 1863
Basal-bridging HH; $(a\text{-}b)_2$ $(dppv)_2$	1930; 1839
Apical-bridging HH; (a-b)(b-b) $(dppv)_2$	1930; 1864
D1D Basal-bridging DD; dppv: (a-b)(b-b) $(dppv)_2$	1922
$Fe_2(pdt)(CO)_2(dppv)_2$ species	***DFT/BP86/TZVP IR (CO stretching region; cm^{-1})***
$(^{12}CO)_2$; $(a\text{-}b)_2$ $(dppv)_2$	1886; 1899
$(^{12}CO)(^{13}CO)$; $(a\text{-}b)_2$ $(dppv)_2$	1848; 1893
$(^{13}CO)(^{13}CO)$; $(a\text{-}b)_2$ $(dppv)_2$	1841; 1855
$(^{12}CO)_2$; (a-b)(b-b) $(dppv)_2$	1891; 1899
$(^{12}CO)(^{13}CO)_{basal}$; (a-b)(b-b) $(dppv)_2$	1847; 1849
$(^{13}CO)_{apical}(^{12}CO)$; (a-b)(b-b)($dppv)_2$	1854; 1892

Appendix on $[HFe_2(pdt)(CO)_3(NCMe)(dppv)]BF_4$

Synthesis of $[HFe_2(pdt)(CO)_3(NCMe)(dppv)]BF_4$. A solution of $[HFe_2(pdt)(CO)_4(dppv)]BF_4$ (163 mg, 0.2 mmol) in 10 mL CH_2Cl_2/MeCN (v/v = 9/1) in a Pyrex tube was irradiated by a 500 W high-pressure Hanovia mercury lamp. A glass filter was used to cut off light below 440 nm. The reaction was monitored by IR spectroscopy, specifically the loss of CO bands of $[HFe_2(pdt)(CO)_4(dppv)]BF_4$ at 2100, 2053, 2038 and 1979 cm^{-1}.[1,2] Over the course of 60 min., the color of the solution changed from dark red to green. The solution was concentrated under vacuum, and the product was precipitated as green powder upon the addition of 20 mL of hexane. Yield: 144 mg, 87%. Single crystals were grown by slow diffusion of hexanes into a CH_2Cl_2 solution. ^1H NMR (CD_2Cl_2): δ 8.63-8.52 (m, 2H, PC*H*), 7.79-7.25 (m, 20H, C_6H_5), 3.05 (m, 2H, SCH_2), 2.76 (m, 2H, SCH_2), 2.45 (m, 2H, SCH_2CH_2 CH_2S), −25.6 (t, 1H, Fe-*H*, J_{PH} = 24 Hz). ^{31}P NMR (CD_2Cl_2): δ 90.5. FT-IR (THF, ν_{CO}): 2079, 2025, 2012 cm^{-1}.

References

1. Barton, B. E.; Zampella, G.; Justice, A. K.; De Gioia, L.; Rauchfuss, T. B.; Wilson, S. R. *Dalton Trans.*, **2010**, *39*, 3011.
2. Wang, W.; Rauchfuss, T. B.; Bertini, L.; Zampella, G. *J. Am. Chem. Soc*. **2012**, *134*, 4525.

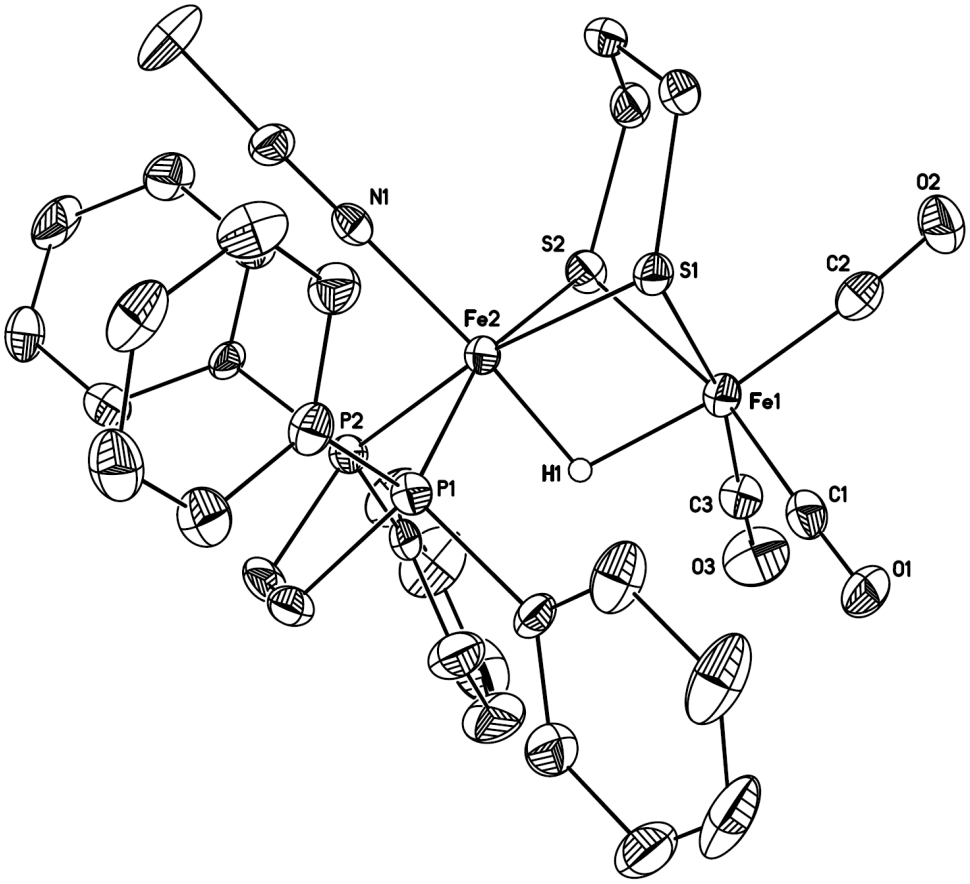

Figure S39. Structure of the cation in $[HFe_2(pdt)(NCMe)(CO)_3(dppv)]BF_4$ showing 30% thermal ellipsoids.

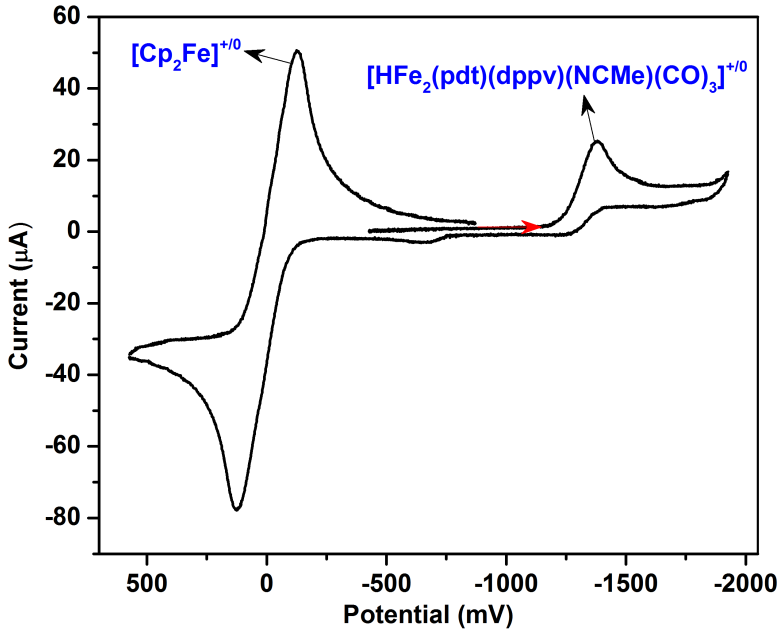

Figure 40. Cyclic votammograms for $[HFe_2(pdt)(dppv)(NCMe)(CO)_3]BF_4$ in CH_2Cl_2 solution. *Conditions:* 1.0 mM $[HFe_2(pdt)(dppv)(NCMe)(CO)_3]BF_4$, 100 mM $[Bu_4N]PF_6$ in, 25 °C, 0.1 V/s scan rate, referenced to $Fc^{+/0}$ (ca. 3 mM). *Results:* the reduction potential of $[HFe_2(pdt)(dppv)(NCMe)(CO)_3]^{+/0}$ is -1.38 V vs. $Fc^{+/0}$ couple.

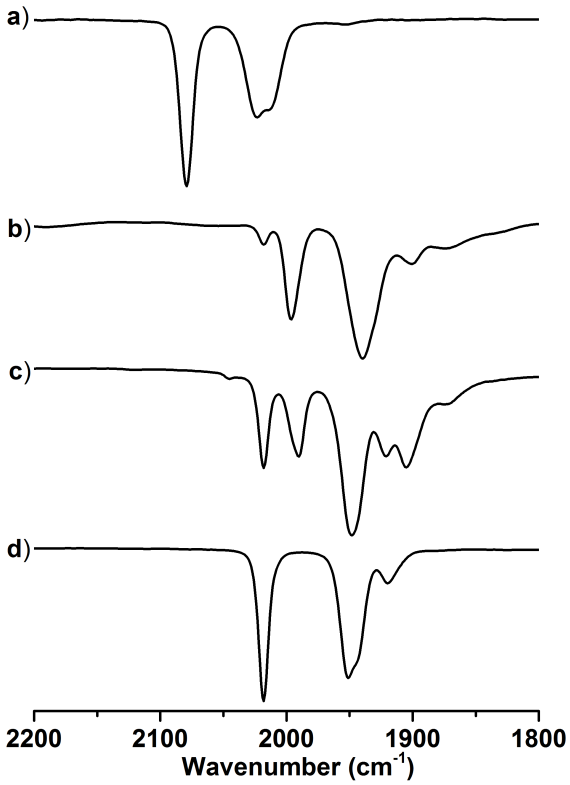

Figure 41. IR spectra (THF solution):

(a) $[HFe_2(pdt)(NCMe)(CO)_3(dppv)]BF_4$ (ν_{CO}: 2079, 2025, 2012 cm^{-1});

(b) Treated $[HFe_2(pdt)(NCMe)(CO)_3(dppv)]BF_4$ with 1 equiv of $[NBu_4]BH_4$ salt after 5 min in THF. New bands appear at 1997, 1939, 1900 cm^{-1};

(c) The reaction mixture of (b) was at room temperature for 3 hours. The intensity of bands at 1997, 1939, 1900 cm^{-1} decreased and the bands at 2018, 1949, 1922 cm^{-1} appear;

(d) authentic sample of $Fe_2(pdt)(CO)_4(dppv)$ with ν_{CO} = 2018, 1949, 1922 cm^{-1}.

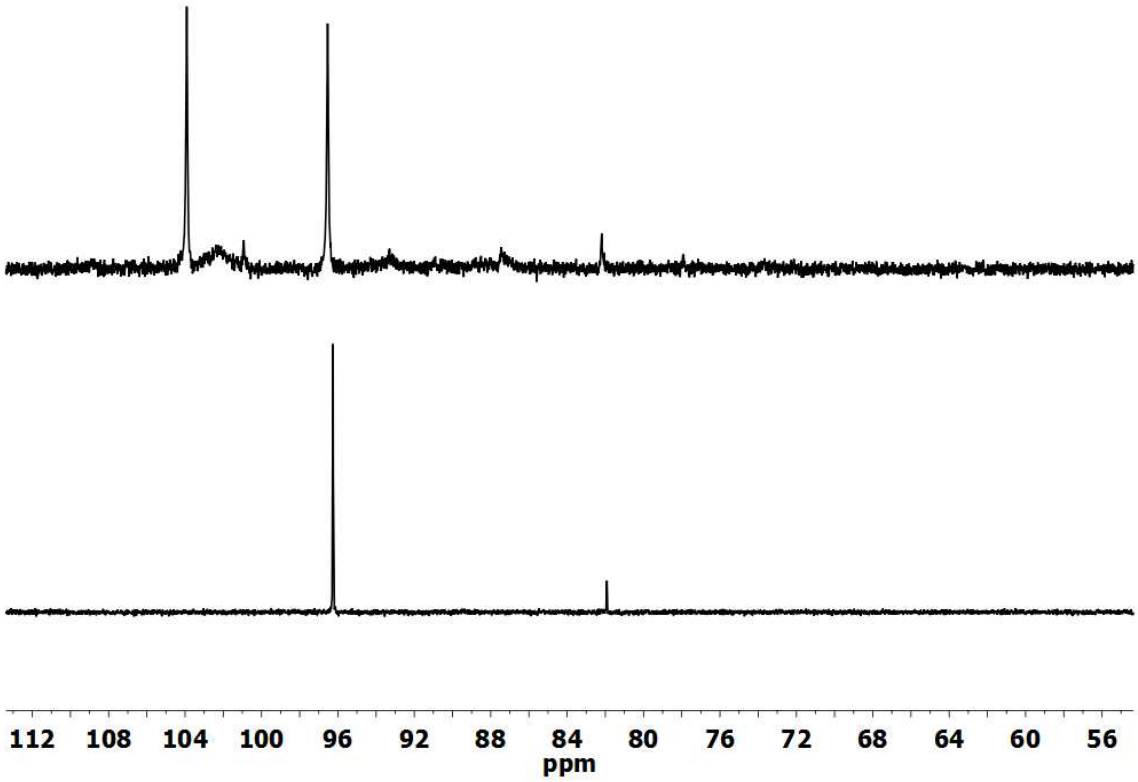

Figure S42. ^{31}P NMR spectra (THF solution):
(*up*): the reaction mixture of $[HFe_2(pdt)(NCMe)(CO)_3(dppv)]BF_4$ with 1 equiv of $[NBu_4]BH_4$ at room temperature for 3 hours (the same solution in Figure S27 (c)). ^{31}P NMR signals at δ 96.5 and 82.2 are assigned to apical-basal, and dibasal isomer (isomer ratio is 90:10) of $Fe_2(pdt)(CO)_4(dppv)$ respectively; other signals, including the one at δ 103.9 are unidentified.
(*bottom*): authentic sample of $Fe_2(pdt)(CO)_4(dppv)$ with ^{31}P NMR signals at δ 96.5 (apical-basal) and 82.2 (dibasal); the two isomer ratio is 90:10.

Combined with the IR spectra, The reaction of $[HFe_2(pdt)(dppv)(CO)_3(NCMe)]BF_4$ with NBu_4BH_4 gives $Fe_2(pdt)(dppv)(CO)_4$ with about 50% yield from ^{31}P NMR spectra and other unknown compounds.